





This is to certify that the

thesis entitled

Effects of Mistuning on the Performance of Centrifugal Pendulum Vibration Absorbers

presented by

Vishal Garg

has been accepted towards fulfillment of the requirements for

M.S. ____degree in Mechanical Engineering

2/18/96

MSU is an Affirmative Action/Equal Opportunity Institution

O-7639

PLACE IN RETURN BOX to remove this checkout from your record. TO AVOID FINES return on or before date due.

DATE DUE	DATE DUE	DATE DUE

MSU is An Affirmative Action/Equal Opportunity Institution cycle/datedus.pm3-p.1

OF CENTRIFUGAL PENDULUM VIBRATION ABSORBERS

 $\mathbf{B}\mathbf{y}$

Vishal Garg

Thesis

Submitted to
Michigan State University
in partial fulfillment of the requirements
for the degree of

MASTER OF SCIENCE

Department of Mechanical Engineering
Michigan State University
East Lansing, MI

ABSTRACT

OF CENTRIFUGAL PENDULUM VIBRATION ABSORBERS

By

Vishal Garg

Torsional vibrations in IC engines are known to cause fatigue and NVH related difficulties. In this thesis, the use of centrifugally driven pendulum absorbers for the attenuation of torsional vibrations is investigated. In particular, the effects of mistuning and nonlinearities on the performance of the absorbers is considered in detail. The model employed is a simple two degree-of-freedom system that includes a rotor and an absorber mass that rides along a quite general path relative to the rotor. Analytical and computational approaches are undertaken to capture the model dynamics for a wide range of path types, in order to evaluate their effectiveness in reducing torsional vibrations of the rotor. The path types considered utilize a general mistuning of their linearized behavior along with a parameter that allows one to vary their large-amplitude character. The results show that overtuned paths generally perform better than undertuned paths. Perfectly tuned cycloids are found to perform best overall among perfectly tunued paths, whereas the perfectly tuned circular path performed the worst. When mistuning is taken into account, it is found that slightly overtuned circular path absorbers offer overall satisfactory performance, and they have the advantage of being simple to implement in practice. The comparison between the numerical and the analytical approaches was generally very accurate. Hence, the analytical results presented herein can be used to provide valuable guidelines for initial design and evaluation of absorber systems.

ACKNOWLEDGEMENTS

I wish to express my sincere gratitude to my thesis advisor Dr. Steven W. Shaw. His timely guidance, advice and suggestions through out the duration of this work is greatly appreciated. I especially thank him for his endless help during the last few months of this work. It has been a great privilege to work with him.

My special thanks to Prof. Alan G. Haddow and Prof. Brian Feeny for agreeing to serve as my committee members and Dr. C. T. Lee, Mr. C. P. Chao for providing many insightful discussions on various topics.

I would also like to thank Dr. S. Kudapa for his friendship and constant encouragement.

Finally, I reserve my deepest and most sincere gratitude to my family members: my parents (Dr. B. Kumar and Rajrani), my brother (Gaurav Garg) for their endless sacrifices.

TABLE OF CONTENTS

L	LIST OF FIGURES		vi
1	Inti	roduction	1
	1.1	Background and History	2
	1.2	Motivation for the Present Work	5
	1.3	Organization of the Thesis	6
2	Ma	thematical Model	7
	2.1	Simplified Model	7
	2.2	Equations of Motion	9
		2.2.1 Nondimensionalization	11
	2.3	Generalized Absorber Path	12
		2.3.1 Mistuning Parameter	17
3	Per	turbation Analysis	20
	3.1	Procedure	20
	3.2	Absorber Paths	21
		3.2.1 K_4 - λ Relationship	22
	3.3	Steady-State Response	23
	3.4	Jump Analysis	25
	3.5	Numerical Examples	28
		3.5.1 Numerical Examples of the Steady-State Results	28
		3.5.2 Numerical Examples for the Jump Phenomenon	34
4	Nu	merical Analysis	42
	4.1	Introduction - Optimization Methodology	42
		4.1.1 Optimization Set-Up	44
	4.2	State Equations	46
	4.3	Statement of Optimization Problem (in Standard Form)	48
	4.4	Numerical Results	49

		4.4.1	General Observation of the Response	49		
		4.4.2	Perfectly Tuned Dynamics	51		
		4.4.3	Mistuned Dynamics	54		
	4.5	Pertu	rbation -Numerical Comparisons	63		
5	Disc	cussion	and Future Direction for Research	68		
	5.1	Design	Guidelines	68		
		5.1.1	Tuned Path Designs	6 8		
		5.1.2	Mistuned Path Designs	69		
		5.1.3	Dynamic Response	70		
	5.2	Limita	ations and Future Work	71		
A	Der	ivation	n of Linear Solution	74		
	A.1	Linear	ization in s and $ heta$	74		
	A.2	Linear	Solution	75		
В	Stat	te equa	ations for the model	77		
Bl	BIBLIOGRAPHY					

LIST OF FIGURES

2.1	Schematic diagram for the CPVA and the rotor from the cross-section view.		8
2.2	Pendulum path in a coordinate system relative to carrier center of		
	rotation	13	
2.3	Generalized absorber paths in intrinsic one-parameter λ form, for $m =$		
	$2, R_0 = 1. \ldots $	15	
2.4	Mistuned absorber paths for $\lambda = 0.6$, for $m = 2$, $R_0 = 1 \dots \dots$	18	
3.1	Performance of the zero-mistuned absorber paths; Peak angular accel-		
	eration vs torque	29	
3.2	Performance of the mistuned $\lambda = 0,0.6$ paths – acceleration versus		
	torque	31	
3.3	Performance of the mistuned $\lambda = 0.8944, 1$ paths- acceleration vs torque.	32	
3.4	Mistuning performance at $\Gamma_n = 0.6, 0.4 \ldots$	35	
3.5	Mistuning performance at $\Gamma_n = 0.2 \ldots \ldots \ldots \ldots$	36	
3.6	Absorber amplitude s_a versus Γ_n at different path λ values	36	
3.7	Performance of the mistuned $\lambda = 0, 0.6$ paths. Absorber amplitude vs		
	torque level	39	
3.8	Performance of the mistuned $\lambda = 0.8944, 1$ paths. Absorber amplitude		
	vs torque level	40	
3.9	Jump torque Γ_J versus mistuning σ at different λ path values	41	
4.1	General absorber response for cycloid and cicular paths- acceleration		
	vs θ	50	
4.2	General Absorber Response for Cycloid and Cicular paths- Absorber		
	Amplitude vs θ	52	
4.3	$ heta$ - Response of perfectly tuned circular paths $\dots \dots \dots \dots$	55	
4.4	θ - Response of perfectly tuned $\lambda=0.6$ paths	56	
4.5	$ heta$ - Response of perfectly tuned epicycloid paths $\dots \dots \dots \dots$	57	
4.6	heta - Response of tuned cycloid paths	58	
4.7	θ - Response of mistuned $\lambda = 0$ (circle) paths	59	

4.8	θ - Response of mistuned $\lambda = 0.8944$ (epicycloid) paths	60
4.9	θ - Response of mistuned $\lambda = 1$ (cycloid) paths	61
4.10	Maximum amplitude of rotor acceleration, $\max(\ddot{\theta})$ versus Γ_n ; solid	
	lines are from perturbation; "o" are from numerical results	64
4.11	Maximum absorber amplitude, $\max(s_a)$ versus Γ_n ; solid lines are from	
	perturbation; "o" are from numerical results	66
4.12	Acceleration, $\ddot{\theta}$ vs θ ; solid lines are from perturbation; "o" are from	
	numerical results	67

CHAPTER 1

Introduction

Centrifugal Pendulum Vibration Absorbers (CPVA's) are used to reduce torsional oscillations in rotating machinery. The reduction of torsional vibrations is important in many applications because they are a source of noise and vibration and they also can reduce the fatigue life of components. A CPVA is essentially a moveable counterweight that is designed to dynamically counteract applied torque excitations of a given order over a range of operating speeds and torque amplitudes. (The order of the excitation referred to here is the number of excitation cycles encountered in each revolution of the rotating shaft on which the absorbers are mounted.) CPVA's have been successfully employed in internal combustion engines and helicopter rotors. In this thesis we choose a simple CPVA model problem in order to investigate certain aspects of the nonlinear dynamic response of absorber systems. We describe the influence of various system parameters, in particular, the parameters that fix the path of the absorber CG, on the overall system response. The results of this study offer an improved understanding of the effectiveness of absorber systems in reducing torsional vibrations and also provide specific information pertaining to the design of CPVA systems.

1.1 Background and History

Background

A CPVA is essentially a mass which is restricted to move along a prescribed path relative to the base rotating system. It is driven by the centrifugal field of the rotating system and provides a torque which can be designed to counteract components of disturbance/applied torques acting on the system. Since the centrifugal force acting on the mass is proportional to the square of the rotating speed, the natural frequency of the CPVA, and thus the frequency which can be accessed for absorption, varies linearly with the rotation speed. This means that once a CPVA is properly tuned to a given harmonic of the nominal rotation speed, that is, for a given order, it will remain effective over a continuous range of rotational speeds. This feature is very useful since many sources of vibrations, such as those arising from inertia and gas pressure effects in IC engines, are dominated by harmonics of the rotation speed.

Other devices that are used to control torsional vibrations include torsional friction dampers, flywheels and conventional tuned vibration absorbers. Torsional friction dampers consume energy and generate heat; flywheels increase the mass and rotational inertial of the system, thereby reducing system responsiveness; and conventional tuned vibration absorbers use elastic elements that can be tuned only to single frequency and are therefore not useful except at a specific rotation rate (in fact, they may have detrimental effects at other rotation rates). CPVAs offer many advantages over these devices. They can often be implemented without increasing the overall mass of the system, or its rotational inertia. When properly designed, they dissipate an insignificant amount of energy in the form of heat and they are effective over a wide range of rotational speeds and torque levels.

A CPVA is characterized by its mass, path shape, and location. Geometric constraints and balancing issues often limit the choice of mass and location for a CPVA.

In that case, the path shape becomes the most important design variable. The most commonly used paths are circles. However, circles mistune at moderate torque amplitudes due to nonlinear effects and can undergo an undesireable jump behavior. Other path types used are cycloids and epicycloids. Certain epicycloids have a special tautochronic property, that is, they have a constant period of oscillation for all amplitudes of motion when operating in a constant-speed centrifugal field [1]. In this thesis we systematically investigate a family of paths for CPVA's that includes all of the above as special cases.

History

Some parts of this section have been directly taken from the review chapter on CPVA's by Shaw and Lee [2].

A thorough account of the history of the CPVA up through the 1960's, including several applications, can be found in Ker Wilson [3] and DenHartog [4]. The first sound technical discussion on CPVA's was published by Miessner at a conference at Stockholm in 1930 (as referenced in Ker Wilson [3]). His experiments demonstrated the effectiveness of such devices and opened the way for intensive development of practical forms of CPVA's. In 1938 Den Hartog published a paper regarding the dynamics of the CPVA at moderate amplitudes of oscillation and pointed out the shortcomings that can occur if one uses purely linear tuning to design the absorber path [5]. Many forms of CPVAs were proposed and patented in Europe during the 1930's and 1940's. Taylor introduced the CPVA to the United States in 1936, and Chilton was the first to build a CPVA in the United States [6, 7]. The Sulzar brothers adapted CPVA's for use on trains and automobiles in the 1930's and 1940's, and achieved very good results. Today, CPVA's are applied in the aircraft/helicopter industry [6, 8, 9] and recently have been tried in experimental automotive applications [10, 11, 12].

Circular paths have been widely used for the CPVA because of their simple implementation and effectiveness at small amplitude oscillations. Meissner provided the geometric relationships for achieving the correct linear tuning frequency using circular paths. Den Hartog extended these results to include the effects of small damping and nonlinearity [5]. Nonlinear mistuning has been observed in experiments and simulations for moderate amplitude vibrations [13, 14, 15]. More complete nonlinear analysis of the undamped system, both for free oscillations [16] and for forced oscillations [13, 17, 18], have been carried out in order to determine the source of the failure of the linear analysis. Newland and Den Hartog [5, 13] suggested intentionally mistuning the linearized system in order to produce favorable tuning at moderate amplitudes of oscillation. It was not until quite recently that possibilities offered by using non-circular paths were explored.

Absorber paths other than circles are possible due to the development of bifilar constructions that use machined paths and rollers [3, 4, 11]. The idea behind these paths is that they reduce the mistuning problems associated with circular paths. Madden [19] was awarded a patent for CPVA's on helicopter rotors which employed cycloidal paths for the absorbers. A cycloid was chosen by Madden, presumably, since it is tautochronic (i.e., its period of motion is independent of amplitude) in a gravitational field. However, a certain epicycloid is known to be tautochronic in a radial centrifugal field [20]. This motivated a study, sponsored by Ford Motor Company, which implemented epicycloidal paths on a four-cylinder, in-line, four-stroke engine. The papers by Denman, Cronin and Borowski et al. [10] describe various aspects of this effort which showed a 92% reduction in the second order oscillation amplitude at the rated torque of this 2.5 L engine, as compared to the engine without absorbers.

1.2 Motivation for the Present Work

The basic desirable feature of the CPVA is that it remains effective, essentially by staying in tune, over a continuous range of rotational speeds. This argument is based on the dynamics of the linearized system, in which the absorber mass does not move far from its equilibruim state. At moderate amplitudes of oscillation, absorbers are known to have the potential to fail miserably [14, 13]. Possible causes for these failures are:

- (1) The absorber frequency is generally dependent on its amplitude of motion and this mistunes the absorber significantly at moderate amplitudes. This may even cause a disastrous jump in the system response as the torque level is increased.
- (2) Each absorber is designed to counteract only a single frequency disturbance and higher harmonics may be amplified through nonlinear effects, thus leading to reduced effectiveness of the absorber. (This can be addressed by employing several absorbers which are tuned to selected harmonics [10, 11].)

Note that these causes are directly linked to nonlinear dynamic effects. In this thesis we will study the effects of modifying the absorber path both at moderate amplitudes, by using cycloids, etc., and at small amplitudes, by intentionally mistuning the absorbers at the linear response level. In this way a direct comparison can be made about the merits and drawbacks of the approaches currently used and, furthermore, new parameter regions can be explored for potential designs.

Therefore, the purpose of this thesis is to investigate the overall system dynamics as a function of the following primary design variables, referred to herein as the path parameters:

- the level of intentional linear mistuning, described by a percentage of mistuning,
 and,
- the large-amplitude path shape, specified herein by using a one-parameter fam-

ily of paths varying from a circle to a cycloid, as developed by Denman [11].

The dynamic analysis contained herein is carried out in two ways. First, a perturbation analysis is performed that captures the nonlinear effects in an analytical manner. These results are then backed up by a systematic numerical study for a given case.

1.3 Organization of the Thesis

This thesis is arranged as follows. The description of the model employed, the equations of motion describing the dynamics of the model and the path parametric equations are provided in Chapter 2. Chapter 3 describes the analytical method employed to obtain approximate solutions of the model equations. Specific numerical examples demonstrating the main results of the analytical study and describing the effects of various important system parameters on the response are also presented. Chapter 4 describes the numerical methodology employed to solve the model equations, and numerical simulation results are also given to describe the effects of system parameters on the response. Comparisons with the analysis are also considered in Chapter 4. A summary, a discussion of the limitations of the current study, and some directions for future research are provided in Chapter 5. Some detailed derivations and a summary of the simulation routine are provided in the appendices.

CHAPTER 2

Mathematical Model

In this chapter we describe the model employed and derive the equations which govern its dynamics. The description of the simplified model employed for the CPVA is provided first. Next, the differential equations which describe the dynamics of the CPVA are derived by Lagrange's method and then nondimensionalized. The equations used to describe the generalized path curve followed by the absorber center of mass are then derived. Also, the definition of the mistuning and nonlinearity parameters associated with this family of paths is included. This provides a complete set of equations which are studied in subsequent chapters.

2.1 Simplified Model

In order to provide some insight into the effects of absorber path curves on the steady state motion of a rotational system, it is necessary to understand the basic operation of the CPVA. A CPVA consists of an absorber mass which is driven by the centrifugal field of the rotational motion in such a manner that its center of mass is restricted to move along a prescribed path relative to the rotor. The motion of this mass provides a torque which can be designed to counteract the disturbance torque, thus smoothing out torsional vibrations.

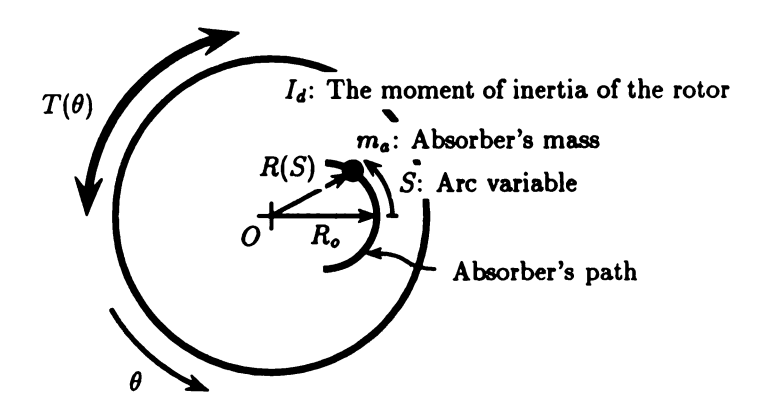


Figure 2.1. Schematic diagram for the CPVA and the rotor from the cross-section view.

The simplified model employed is shown in Figure 2.1. It consists of a rigid disk and a point mass m_a for the absorber riding on a prescribed path relative to the disk. The disk is called the carrier, and it represents the rotational inertia of the system I_d (for example a crankshaft or a helicopter rotor); its orientation is given by θ . The absorber mass rides on the prescribed path which is specified by a function of its position relative to the carrier. The disk is subjected to an external torque $T(\theta)$, which is assumed to be of the form $T(\theta) = T_n \sin n\theta$, n representing the dominant harmonic that occurs in the rotational system. Due to symmetry of the applied torque, the absorber path is chosen to be symmetric about its vertex [21]. (The vertex is defined to be the point on the absorber path which is furthest from the carrier center of rotation O). From the vertex, an arc length variable S is assigned to specify the location of the absorber mass along the path, that is, S = 0 at the vertex; see Figure 2.1. The distance from a point on the path to point O is denoted as R, and R is expressed as a function of S, that is, R = R(S). The path is uniquely determined once R(S) is chosen. The value of R at the vertex is denoted as R_0 , that is, $R_0=R(0)$. The absorber has a nominal moment of inertia of $I_1=m_aR_0^2$ about point O. The damping for the disk and the absorber are ignored in this study. (This assumption is significant, but valid for initial design evaluations, as one must keep the absorber damping small in order to achieve satisfactory performance). The nominal speed of the disk is Ω , while the oscillating torque is the source of speed fluctuations about Ω .

2.2 Equations of Motion

The equations of motion are determined by Lagrange's method. For the generalized coordinates which describe the configuration of the system we choose S, the arclength parameter along the absorber CG path, and θ , the angular orientation of the disk relative to an inertial frame of reference. The total kinetic energy of the system can be divided into the kinetic energy of the disk and that of the absorber.

The kinetic energy of the disk is given by $\frac{1}{2}I_d\dot{\theta}^2$ where $\dot{\theta}$ is the rotation rate of the disk. The kinetic energy of the absorber is given by $\frac{1}{2}m_a\vec{V_a}\cdot\vec{V_a}$ where $\vec{V_a}$ is the velocity of the CG of the absorber. The velocity, V_a , is given by

$$V_a = R\dot{\theta}\vec{e_\theta} + \dot{S}\vec{e_S} \tag{2.1}$$

where $\vec{e_{\theta}}$ is a unit vector along circumferential direction of the disk rotation at the absorber location and $\vec{e_{s}}$ is a unit vector tangent to the path direction at that point. From the geometry of the path, the inner product $\vec{e_{\theta}} \cdot \vec{e_{S}}$ is given by $R\frac{d\phi}{dS}$ where dS is the differential of S, and $d\phi$ is the angle expanded by dS from the disk rotation center. The parameters, dS, dR and $d\phi$ are related by the following geometric constraint on the arclength,

$$(dS)^{2} = (dR)^{2} + (Rd\phi)^{2}, \tag{2.2}$$

which leads to

$$\frac{d\phi}{dS} = \frac{1}{R} \sqrt{1 - \left(\frac{dR}{dS}\right)^2},\tag{2.3}$$

where the positive sign is chosen for the square root in the above equation since ϕ is assumed to increase with S. Therefore,

$$\vec{e_{\theta}} \cdot \vec{e_{S}} = \sqrt{1 - \left(\frac{dR}{dS}\right)^2} \tag{2.4}$$

The translational part of the kinetic energy of the absorber is then given by

$$\frac{1}{2}m_{a}\vec{V_{a}} \cdot \vec{V_{a}} = \frac{1}{2}m_{a}\left(R^{2}\dot{\theta}^{2} + \dot{S}^{2} + 2R\dot{\theta}\dot{S}\vec{e_{\theta}}.\vec{e_{S}}\right) \\
= \frac{1}{2}m_{a}(X\dot{\theta}^{2} + \dot{S}^{2} + 2\dot{\theta}\dot{S}G) \tag{2.5}$$

where $X = X(S) = R^2(S)$, and $G = G(S) = \sqrt{X - \frac{1}{4}X'^2}$ where ()' denotes the derivative with respect to S.

We can now write down the total kinetic energy of the system, K_E , which is given by

$$K_E = \frac{1}{2} (I_d) \dot{\theta}^2 + \frac{1}{2} m \vec{V_a} \cdot \vec{V_a}$$

$$= \frac{1}{2} (I_d) \dot{\theta}^2 + \frac{1}{2} m (X \dot{\theta}^2 + \dot{S}^2 + 2 \dot{\theta} \dot{S} G)$$
(2.6)

Assuming that gravitational effects are small, there are no forces derivable from potential energy.

For determining the equations of motion, Lagrange's equations of motion are applied:

$$\frac{d}{dt}\left(\frac{\partial L}{\partial \dot{q}_i}\right) - \frac{\partial L}{\partial q_i} = Q_i' \tag{2.7}$$

where, for the assumptions stated above,

$$L = K_E$$
$$q_i = \{\theta, S\}$$

$$Q_i' = \{T(\theta), 0\}$$

which results in the following equations of motion for the system

$$(I_d)\ddot{\theta} + m_a \left(X\ddot{\theta} + X'\dot{\theta}\dot{S} + G\ddot{S} + G'\dot{S}^2 \right) = T(\theta)$$

$$\ddot{S} + G\ddot{\theta} - \frac{1}{2}X'\dot{\theta}^2 = 0$$
(2.8)

Note that m_a simply divides out of the second equation.

2.2.1 Nondimensionalization

It is convenient to present the equations of motion in dimensionless form. By nondimensionalizing, the number of parameters associated with the equation of motion is reduced. In order to nondimensionalize the equations of motion, we rescale by defining the following dimensionless quantities:

$$s = \frac{S}{R_0}$$

$$\tau = \Omega t$$

$$\dot{(\cdot)} = \frac{d(\cdot)}{d\tau}$$

$$x(s) = \frac{R^2(R_0 s)}{R_0^2}$$

$$g(s) = \sqrt{x(s) - \frac{1}{4} \left(\frac{dx(s)}{ds}\right)^2}$$

$$b_0 = \frac{I_d}{I_1}$$

$$\Gamma_n = \frac{T_n}{I_1 \Omega^2} = \frac{T_n}{m_a R_0^2 \Omega^2}$$

Note that we have redefined the overdot. The equations of motion in terms of these parameters are given by

$$\ddot{s} + g(s)\ddot{\theta} - \frac{1}{2}\frac{dx}{ds}(s)\dot{\theta}^2 = 0,$$
 (2.9)

$$b_0\ddot{\theta} + \frac{dx}{ds}(s)\dot{s}\dot{\theta} + x(s)\ddot{\theta} + g(s)\ddot{s} + \frac{dg}{ds}(s)\dot{s}^2 = \Gamma_n \sin n\theta \qquad (2.10)$$

If the disk never reverses its direction, e.g., $\dot{\theta} > 0$ always, then any function of τ can be expressed a as function of θ , which makes possible a switch of the independent variable from τ to θ . Note that with this change the angular speed of the disk is treated as a variable dependent on θ , denoted as $y = \dot{\theta}(\theta)$. Defining (·)' as $\frac{d(\cdot)}{d\theta}$, the equations of motion become

$$ys'' + (s' + g(s))y' - \frac{1}{2}\frac{dx}{ds}(s)y = 0,$$

$$g(s)y^{2}s'' + (b_{0} + x(s) + g(s)s')yy' + \frac{dx}{ds}(s)s'y^{2} + \frac{dg}{ds}(s)s'^{2}y^{2} = \Gamma_{n}\sin n\theta, \qquad (2.11)$$

Note that in terms of these variables, the angular acceleration, θ , is equal to yy'. Also, the unforced base operating point for the system is given by $\Gamma_n = 0$, y = 1 and s = 0.

2.3 Generalized Absorber Path

In order to complete the equations of motion, the absorber path followed by the pendulum mass must be specified. Figure 2.2 defines the geometric quantities, that are needed in the development of equations for the generalized path.

In the figure,

• (p,q) are cartesian coordinates defined at carrier centre of rotation.

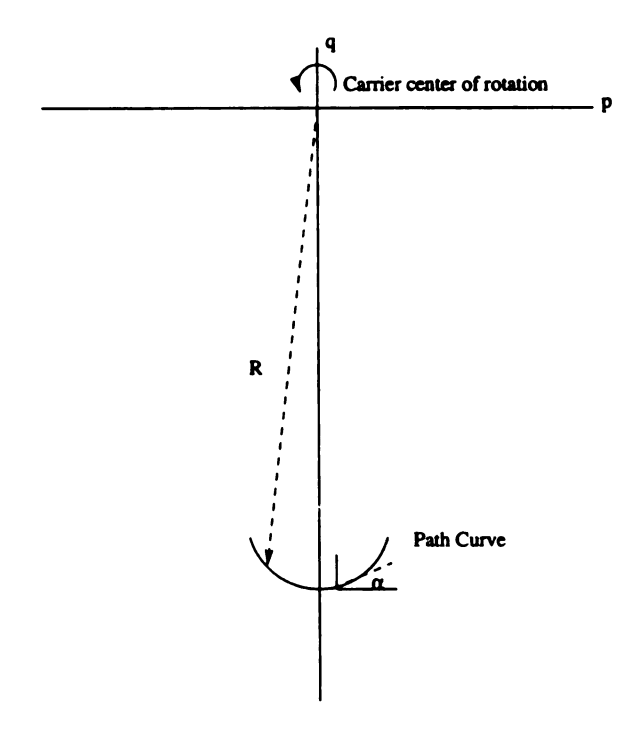


Figure 2.2. Pendulum path in a coordinate system relative to carrier center of rotation

- R is distance from the carrier center of rotation to the point on the path curve where the absorber mass is located and is given by $R(S) = p^2(S) + q^2(S)$. Note that the coordinates have been parameterized in arc length variable, S.
- α , defines the slope of the path curve with respect to the p axis, where $\alpha = \tan^{-1} dq/dp$
- ρ is the local radius of curvature of the path curve, where $\rho = (1 + q'^2)^{3/2}/q''$, here ()' = d()/dp.
- S=0 is the vertex of the path curve, which is taken as symmetric about the q axis; thus, at s=0: $\alpha=0$, dq/dp=0 and p=0.
- $q=-R_0$ at S=0.

The generalized curve represents a family of curves that in intrinsic one-parameter form is given by,

$$\rho^2 = \rho_0^2 - \lambda^2 S^2, \tag{2.12}$$

where ρ_0 is the radius of curvature at the vertex and λ is used to specify the nonlinear character of the path. Note that this form is not the most general, but it contains the most common paths employed. The constant ρ_0 sets the frequency of small oscillations for the system, and if set as

$$\rho_0 = -R_0/(m^2 + 1) \tag{2.13}$$

it provides the tuning required to cancel an order m torque in the linear range.

The λ parameter values of interest are in the range $\lambda \in [0,1]$, where $\lambda = 0$ gives a circle, $\lambda = 1$ is a cycloid, and $\lambda^2 = m^2/(m^2 + 1)$ is an epicycloid with its base circle of radius $(R_0 - \rho_0)$ centered at the disk center. Other values of λ correspond to epicycloids scaled by a factor $\rho_0/R_0^2(1-\lambda^2)$ and then translated vertically until their vertices are at $(0, -R_0)$ [11].

A hypocycloid family of curves corresponds to $\lambda > 1$. Only hypocycloids close to the cycloid curves are considered, as those corresponding to large values of λ result in smaller arclength between the cusps, thus limiting the pendulum mass to very small motions. Figure 2.3 shows the family of curves generated for different values of λ as represented by equation (2.2). Note that these curves correspond to the (p,q) coordinate system mentioned earlier. Note also that all paths have a practical limit imposed either by a cusp point or by the point on the path where the centrifugal field will no longer provide the contact force needed to maintain the mass on the path. (Since absorbers are not designed like a "bead on a wire".)

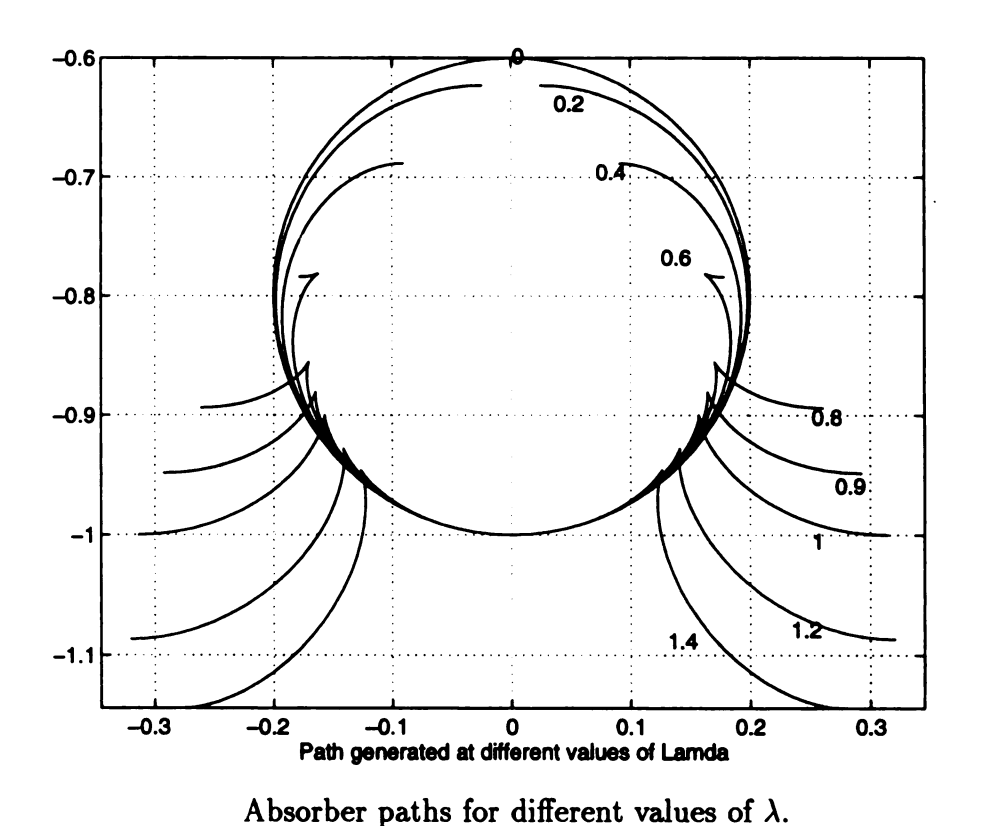


Figure 2.3. Generalized absorber paths in intrinsic one-parameter λ form, for m=2, $R_0=1$.

We now derive some relationships between the various geometric path variables with the ultimate goal of obtaining the function X(S), needed in the equations of motion, in terms of ρ_0 and λ .

Note that

$$\alpha = \int d\alpha = \int_0^S \frac{dS}{\rho} = \int_0^S \frac{dS}{\sqrt{\rho^2 - \lambda^2 S^2}} = \frac{1}{\lambda} \sin^{-1} \frac{\lambda S}{\rho_0}, \qquad (2.14)$$

or

$$S = \frac{\rho_0}{\lambda} \sin \lambda \alpha, \quad \lambda \neq 0; \quad S = \rho_0 \alpha, \quad \lambda = 0.$$
 (2.15)

Also, since

$$p = \int_0^S \cos \alpha dS = \int_0^\alpha \cos \alpha \rho d\alpha, \quad q = R_0 - \int_0^S \sin \alpha dS, \tag{2.16}$$

we obtain, for $\lambda \neq 1$,

$$p = \frac{\rho_0}{1 - \lambda^2} (\sin \alpha \cos \lambda \alpha - \lambda \sin \lambda \alpha)$$

$$q = R_0 + \frac{\rho_0}{1 - \lambda^2} (\cos \alpha \cos \lambda \alpha + \lambda \sin \lambda \alpha \sin \alpha - 1), \qquad (2.17)$$

and, for $\lambda = 1$ (cycloid),

$$p = \frac{1}{2}\rho_0 \left(\alpha + \frac{1}{2}\sin 2\alpha\right),$$

$$q = -R_0 + \frac{1}{4}\rho_0 (1 - \cos 2\alpha).$$
(2.18)

Therefore, we get

$$X = R(S)^2 = p^2 + q^2 (2.19)$$

which using equation (2.17) specifies X(S) as a function of ρ_0 and λ , as required.

Also,

$$X' = 2R\frac{dR}{dS} = 2\left(\frac{\rho_0}{1-\lambda^2} - R_0\right) \sin \alpha - \frac{\lambda^2}{1-\lambda^2}S, \quad \lambda \neq 1,$$

$$X' = \rho_0 \left(\alpha \cos \alpha + \sin \alpha\right) - R_0 \sin \alpha, \quad \lambda = 1$$
(2.20)

Similarly, expressions for G and G' can also be obtained using the definitions in equation (2.5). The functions X, X', G, G' can then be nondimensionalized to obtain x, $\frac{dx}{ds}$, g and $\frac{dg}{ds}$ respectively.

2.3.1 Mistuning Parameter

It is interesting to examine the effect of altering the tuning of the pendulum relative to the order of the dominant harmonic of the disturbing torque. If n is the dominant harmonic of the disturbing torque and m is the order to which the absorber path is designed, then one can define a mistuning parameter σ which is given by the relation

$$n(1+\sigma)=m. \tag{2.21}$$

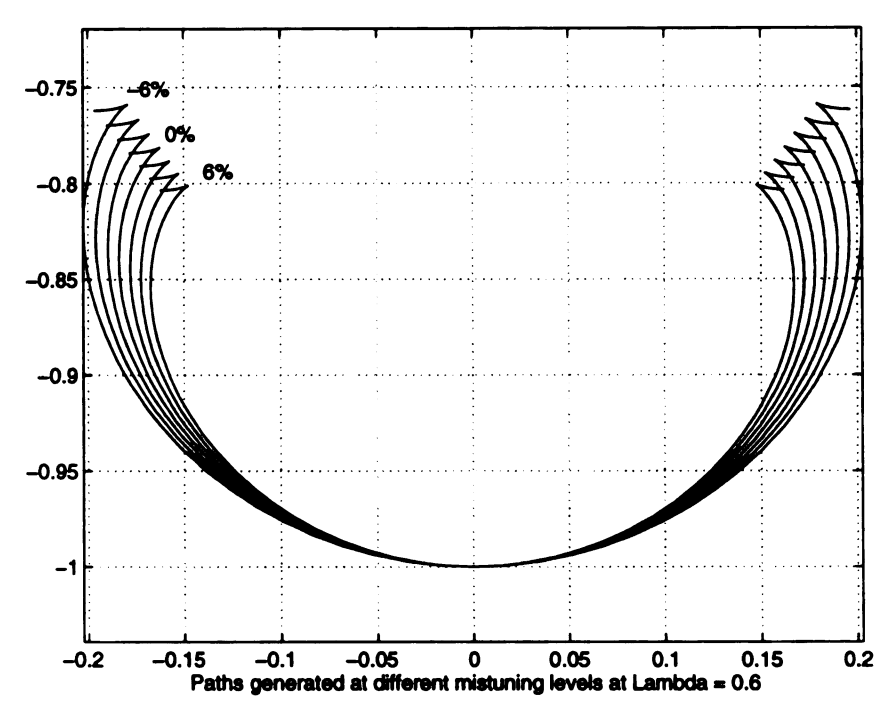
Therefore, ρ_0 from equation (2.13) becomes

$$\rho_0 = -R_0 / \left(n^2 \left(1 + \sigma \right)^2 + 1 \right). \tag{2.22}$$

Figure 2.4 shows the family of curves generated for different values of mistuning at $\lambda = 0.6$ as represented by equation (2.2). The mistuning values are expressed in percentage and are given by

$$\sigma = \{-6\%, -4\%, -2\%, 0\%, 2\%, 4\%, 6\%\}. \tag{2.23}$$

We now have a model by which one can investigate the effects of mistuning (σ)



Absorber paths for different mistuning values at $\lambda = 0.6$.

Figure 2.4. Mistuned absorber paths for $\lambda = 0.6$, for m = 2, $R_0 = 1$

and nonlinearity (λ) on the performance of an absorber.

CHAPTER 3

Perturbation Analysis

In this chapter the analytical method for deriving approximate solutions for the steady-state response to the model equations is described. First, the procedure for developing perturbation solutions for the system is presented. Next, absorber path functions that are suitable for perturbation analysis are formulated. The relationship between these path functions and the general path functions is also presented. Then the steady-state response of the system is described. The solution obtained from linear theory is then derived and used for comparative purposes. The nonlinear solution is obtained next. Finally, results that summarize the analysis are graphically presented and explained for some specific cases of interest.

3.1 Procedure

The following approach is taken for performing the perturbation analysis. The torque Γ_n is assumed to be small, and the two variables s and y are expanded in power series in terms of Γ_n , as follows:

$$s(\theta) = \Gamma_n s_1(\theta) + \Gamma_n^2 s_2(\theta) + \Gamma_n^3 s_3(\theta) + \cdots, \qquad (3.1)$$

$$y(\theta) = 1 + \Gamma_n y_1(\theta) + \Gamma_n^2 y_2(\theta) + \Gamma_n^3 y_3(\theta) + \cdots$$
 (3.2)

Note that the leading term for y is unity since $y \to 1$ as $\Gamma_n \to 0$. Also, all the y_j 's, where $j = 1, 2, \dots$, should oscillate about zero.

This expansion will capture first-order nonlinear effects, but can be quite accurate out to moderate levels of torque. The results obtained are of importance in path design considerations.

The approximate solution is achieved by substituting these expansions for s and y into the equations of motion, (2.11), collecting terms of the same order, and solving for the s_j 's and y_j 's for $j = 1, 2, 3, \cdots$ [21].

3.2 Absorber Paths

Absorber paths are represented by their corresponding path functions. These path functions must be represented as expansions in s in order to perform perturbation analysis. Absorber path functions, in both exact forms and expansions up to order s^4 , are given below for some absorber paths. Note that in each case the curve is chosen so that the curvature at the vertex provides order m tuning in the linear range (recall that the torque is of order n). This implies that each path has the same coefficient at order s^2 .

Circle:

$$x(s) = 1 - \frac{2m^2 \{1 - \cos[(m^2 + 1)s]\}}{(m^2 + 1)^2}$$
$$= 1 - m^2 s^2 + \frac{m^2 (m^2 + 1)^2 s^4}{12} + O(s^6);$$
(3.3)

Cycloid:

$$x(s) = 1 - \left(m^2 + \frac{3}{4}\right) s^2 + \frac{\left\{\sin^{-1}\left[(m^2 + 1)s\right]\right\}^2}{4(m^2 + 1)^2} + \frac{\sin^{-1}\left[(m^2 + 1)s\right]\sin\left[2sin^{-1}\left(m^2 + 1\right)s\right]}{4(m^2 + 1)^2} = 1 - m^2 s^2 - \frac{(m^2 + 1)^2 s^4}{12} + O\left(s^6\right);$$
(3.4)

Tautochronic epicycloid:

$$x(s) = 1 - m^2 s^2; (3.5)$$

General:

$$x(s) = 1 - m^2 s^2 + K_4 s^4 + \cdots, (3.6)$$

where K_4 is a constant such that this form accounts for the first-order nonlinearities in all possible paths [21].

3.2.1 K_4 - λ Relationship

Before evaluating the steady-state response of the system, it is important to obtain a relationship between the path parameters λ and m and the path coefficient K_4 . This relationship can be obtained by expanding $X(S,\lambda)$ in terms of S using equations (2.13) through (2.18), non-dimensionalization, and a direct comparison of the resulting coefficient of s^4 with equation (3.16). The relationship between K_4 and λ and m is found to be

$$K_4 = \frac{(m^2 + 1)^2 (m^2 - \lambda^2 (1 + m^2))}{12}. (3.7)$$

The above relationship is important because it forms the basis for comparing results obtained in this chapter with the numerical results obtained in the next chapter. The

reader should recall that hidden in m is both the order of the applied torque, n, and the level of mistuning, σ . Since n is pre-determined, one can use either (σ, K_4) or (m, λ) as the path design variables, since either pair can be specified.

3.3 Steady-State Response

We take the absorber path to have the general form described by (3.16), and then specialize to specific cases of interest by assigning different values of K_4 and σ . Following the methodology described in the procedure section, the leading order (linear) terms in Γ_n are found to be

$$s_1''(\theta) + m^2 s_1(\theta) + y_1'(\theta) = 0 (3.8)$$

$$s_1''(\theta) + (b_0 + 1)y_1'(\theta) = \sin n\theta, \tag{3.9}$$

which yield the following solution

$$s_1(\theta) = -\left(\frac{\sin n\theta}{m^2 (1+b_0) - b_0 n^2}\right)$$

$$y_1(\theta) = -\left(\frac{(m^2 - n^2) \cos n\theta}{n (m^2 (1+b_0) - b_0 n^2)}\right). \tag{3.10}$$

When the absorber is tuned at linear level such that m = n, the solution is given by

$$s_1(\theta) = -\frac{\sin n\theta}{n^2}, \quad y_1(\theta) = 0.$$
 (3.11)

Note that this is the desired behavior since the rotor runs at a constant speed. If one could insure that amplitudes remained small, this would be a good design. In practice, however, one sees a range of torques and it is impractical to keep amplitudes small in all cases, as this would require either large absorber mass m_a or large moment arm R_0 .

Higher order terms for s and y are determined by straightforward application of the perturbation procedure, yielding

$$s = -\Gamma_n \left(\frac{\sin n\theta}{m^2 (1 + b_0) - b_0 n^2} \right) + \Gamma_n^2 \alpha_0 \sin 2n\theta$$

$$+ \Gamma_n^3 (\alpha_1 \sin n\theta + \alpha_2 \sin 3n\theta) + \cdots, \qquad (3.12)$$

$$y = 1 - \Gamma_n \left(\frac{(m^2 - n^2) \cos n\theta}{n (m^2 (1 + b_0) - b_0 n^2)} \right) + \Gamma_n^2 \alpha_3 \cos 2n\theta$$

$$+ \Gamma_n^3 (\alpha_4 \cos n\theta + \alpha_5 \cos 3n\theta) + \cdots, \qquad (3.13)$$

where

$$\alpha_{0} = \frac{-2m^{4} - 2b_{0}m^{4} + 5b_{0}m^{2}n^{2} - 3b_{0}n^{4}}{2n\alpha_{01}}$$

$$\alpha_{3} = \frac{-m^{6}(1+b_{0}) + m^{4}n^{2}(5+6b_{0}) - m^{2}n^{4}(-2+9b_{0}) + 4b_{0}n^{6}}{4n^{2}\alpha_{01}}$$

$$\alpha_{01} = \left(m^{2} + b_{0}m^{2} - 4b_{0}n^{2}\right) \left(m^{2} + b_{0}m^{2} - b_{0}n^{2}\right)^{2}$$

$$\alpha_{11} = 1 + 2b_{0} + b_{0}^{2}$$

$$\alpha_{1} = \left((-4\alpha_{11})m^{8} + (-12K_{4}\alpha_{11})m^{2}n^{2} + \left(7 + 34b_{0} + 27b_{0}^{2}\right)m^{6}n^{2} + (3\alpha_{11})m^{8}n^{2} + \left(48b_{0}K_{4} + 48b_{0}^{2}K_{4}\right)n^{4} + \left(-8 - 63b_{0} - 71b_{0}^{2}\right)m^{4}n^{4} + \left(-4 - 19b_{0} - 15b_{0}^{2}\right)m^{6}n^{4} + \left(28b_{0} + 68b_{0}^{2}\right)m^{2}n^{6} + \left(16b_{0} + 12b_{0}^{2}\right)m^{4}n^{6} - 20b_{0}^{2}n^{8}\right) / \left(8n^{2}\alpha_{01}\left(m^{2} + b_{0}m^{2} - b_{0}n^{2}\right)^{2}\right)$$

$$\alpha_{2} = \left((-8\alpha_{11})m^{8} + (4K_{4}\alpha_{11})m^{2}n^{2} + \left(-1 + 66b_{0} + 67b_{0}^{2}\right)m^{6}n^{2} + \left(-\alpha_{11}\right)m^{8}n^{2} + \left(-16b_{0}K_{4} - 16b_{0}^{2}K_{4}\right)n^{4}$$

$$(3.14)$$

 $+\left(-59b_0-167b_0^2\right)m^4n^4+\left(4+9b_0+5b_0^2\right)m^6n^4$

 $+\left(-12b_0+168b_0^2\right)m^2n^6\left(-16b_0-4b_0^2\right)-60b_0^2n^8$

 $(8n^2\alpha_{01}(m^2+b_0m^2-b_0n^2)(m^2+b_0m^2-9b_0n^2))$

(3.19)

$$\alpha_{4} = \left((-\alpha_{11}) m^{10} + \left(8b_{0} + 8b_{0}^{2} \right) m^{8} n^{2} + (12K_{4} + 12K_{4}b_{0}) m^{2} n^{4} \right. \\ + \left(3 - 12b_{0} - 22b_{0}^{2} \right) m^{6} n^{4} + \left(-4 - 4b_{0} \right) m^{8} n^{4} - 48b_{0} K_{4} n^{6} \\ + \left(-10 + 20b_{0} + 28b_{0}^{2} \right) m^{4} n^{6} + \left(4 + 20b_{0} \right) m^{6} n^{6} \\ + \left(-14b_{0} - 17b_{0}^{2} \right) m^{2} n^{8} - 16b_{0} m^{4} n^{8} + 4b_{0}^{2} n^{10} \right) / \\ \left(8n^{3} \alpha_{01} \left(m^{2} + b_{0} m^{2} - b_{0} n^{2} \right)^{2} \right)$$

$$\alpha_{5} = \left((-\alpha_{11}) m^{10} + \left(12 + 28b_{0} + 16b_{0}^{2} \right) m^{8} n^{2} + \left(-12K_{4} - 12b_{0} K_{4} \right) m^{2} n^{4} \right. \\ \left. + \left(15 - 60b_{0} - 78b_{0}^{2} \right) m^{6} n^{4} + \left(4 + 4b_{0} \right) m^{8} n^{4} + 48b_{0} K_{4} n^{6} \right. \\ \left. + \left(2 + 24b_{0} + 148b_{0}^{2} \right) m^{4} n^{6} + \left(-12 - 28b_{0} \right) m^{6} n^{6} \right. \\ \left. + \left(\left(34b_{0} - 121b_{0}^{2} \right) m^{2} n^{8} + 48b_{0} m^{4} n^{8} + 36b_{0}^{2} n^{10} \right) / \\ \left. \left(8n^{3} \alpha_{01} \left(m^{2} + b_{0} m^{2} - b_{0} n^{2} \right) \left(m^{2} + b_{0} m^{2} - 9b_{0} n^{2} \right) \right)$$

$$\left. \left(3.21 \right) \right.$$

Using these results, the expansion for the angular acceleration $\ddot{\theta}$ is found to be

$$\ddot{\theta} = yy' = \frac{\Gamma_n (m^2 - n^2) \sin n\theta}{m^2 + b_0 m^2 - b_0 n^2} + \frac{\Gamma_n^2 (-3 (m^4 n + m^2 n^3)) \sin 2n\theta}{2\alpha_{01}} - n\Gamma_n^3 (\alpha_4 \sin n\theta + 3\alpha_5 \sin 3n\theta) + \cdots$$
(3.22)

Note that the n and 2n harmonics in $\ddot{\theta}$ are not affected by K_4 , and $\ddot{\theta}$ is therefore path independent upto order Γ_n^2 . However, as expected, all orders of $\ddot{\theta}$ are affected by m.

The desired result is now in hand: the relationship between angular acceleration, $\ddot{\theta}$, and the path parameters, (σ, K_4) . These can be used for a variety of investigations of system performance.

3.4 Jump Analysis

The jump phenomenon has been observed and documented in analytical studies and in real applications for absorbers using circular paths (Newland, 1964) [13]. This

phenomenon occurs when the amplitude of the absorber motion grows rapidly (even discontinuously) with respect to the torque amplitude Γ_n . This corresponds to the points of vertical tangency in classic nonlinear resonance curves. Jumps can spell disaster for a system, since the response on the upper (that is, large amplitude) solution branch results in a torque generated by the absorber that is generally in phase with the applied torque, causing a dramatic increase in torsional vibration amplitude. The jump analysis also provides additional important information relative to the perturbation results. Specifically, the regular perturbation results as derived above will generally give nice smooth, single-valued response curves as a function of torque amplitude. However, these have a limited range of validity, and the primary limitation is the jump encountered, where the response curve can become multi-valued. Therefore, a bound on the torque range over which the steady-state perturbation results are valid can be approximated by determining the torque level at which a jump occurs.

Mathematically speaking, a jump occurs when $\frac{ds_a}{d\Gamma_n} \to \infty$, where s_a is the amplitude of the absorber motion. However jumps do not occur for all paths, as the absorber amplitude is limited by the fact that g(s) must be real. (At points where g(s) = 0, the absorber point mass reaches a singular point, specifically, a cusp, in the path. In practice, absorbers can not generally achieve such operating levels). Let s_J and s_g be the absorber amplitude at which the jump occurs and the amplitude at which g(s) = 0, respectively. Then a jump can occur only if $s_J < s_g$. This condition is very difficult to check, as estimates of s_j 's are not easily obtained.

We can, however, estimate s_a by noting that in this undamped case s is a series of *sine* harmonics only and that, since the order n sine harmonic is dominant, s reaches its maximum (or minimum) at $\theta = \frac{\pi}{2n}$. This assumption is reasonable as the fundamental harmonic for s_a , which corresponds to the order n harmonic, is quite close to the linear solution of the system, while the remaining harmonics are generated by nonlinear terms, and these remain relatively small for the absorber.

With this assumption, the amplitude s_a is affected by the coefficients of odd order sines only, since all even order sines vanish at $\theta = \frac{\pi}{2n}$. With the order m absorber paths, the amplitude s_a achieved in this way are polynomials in Γ_n , with a leading order term of $s_a \approx \frac{\Gamma_n}{m^2(1+b_0)-b_0n^2}$, which is the solution of the linearized system. In order to calculate s_J the relationship between s_a and Γ_n is inverted so that Γ_n is approximated by a series expansion in terms of s_a . Then, the value of s_J is taken as the value of s_a at which $\frac{d\Gamma_n}{ds_a} = 0$. At this jump point, the corresponding torque amplitude $(\Gamma_n)_J$ is obtained by substituting s_J into the relationship between Γ_n and s_a . The details of these calculations follow.

Following the assumptions outlined above we obtain the approximation

$$s_a = \frac{\Gamma_n}{m^2 (1 + b_0) - b_0 n^2} + \alpha_5 \Gamma_n^3 + \cdots, \tag{3.23}$$

where

$$\alpha_5 = \alpha_2 - \alpha_1. \tag{3.24}$$

The inverse relationship between s_a and Γ_n is obtained by expressing Γ_n as a Taylor series expansion in terms of s_a and matching coefficients at each order, yielding

$$\Gamma_n = \left(m^2 \left(1 + b_0\right) - b_0 n^2\right) s_a - \left(m^2 \left(1 + b_0\right) - b_0 n^2\right)^4 \alpha_5 s_a^3 + \cdots$$
 (3.25)

The jump occurs when $\frac{d\Gamma_n}{ds_a} = 0$, at which point s_J is the corresponding value of s_a , that is, $\frac{d\Gamma_n}{ds_a}(s_J) = 0$. It is thus determined that

$$s_J \approx \frac{1}{\sqrt{3\alpha_5 \left(m^2 \left(1 + b_0\right) - b_0 n^2\right)^3}}.$$
 (3.26)

The corresponding jump torque $(\Gamma_n)_J$ is estimated to be

$$(\Gamma_n)_J \approx \frac{2(m^2(1+b_0)-b_0n^2)}{3\sqrt{3\alpha_5(m^2(1+b_0)-b_0n^2)^3}}.$$
 (3.27)

Note that for jumps to occur, both $g(s_J) > 0$ and $\alpha_5 > 0$ must hold, since both $g(s_J)$ and s_J must be real, where

$$g(s) = \sqrt{1 - m^2 (m^2 + 1) s^2 + K_4 (4m^2 + 1) s^4 + \cdots}.$$
 (3.28)

These results are useful in determining whether a given path is susceptible to the jump behavior. This is crucial in design considerations since, as described above, jumps can wreak havoc on system performance.

3.5 Numerical Examples

Steady-state solutions and the jump phenomenon are investigated for absorber paths varying from a circle to a cycloid for different levels of mistuning. The example considered is from a 2.5 liter four-cylinder, four-stroke engine considered by Denman and Lee and Shaw [1, 21], for which n = 2 and $b_0 = 6.017$. Absorber performance is determined by comparing maximum acceleration levels at different torque amplitudes. The jump phenomenon results from section 3.4 are used to estimate the region of validity of the approximate steady-state solutions obtained from the perturbation solution. The parameters λ and σ will be used to determine the path.

3.5.1 Numerical Examples of the Steady-State Results

Equation (3.22) is used to obtain the angular acceleration, θ of the rotor as a function of θ . The angular displacement, θ , is varied over a one-period interval, $\left[\frac{-\pi}{n}, \frac{\pi}{n}\right]$, and

the absolute maximum acceleration is numerically obtained for given values of λ , σ and Γ_n . Note that the K_4 value required in equation (3.22) can be obtained from equation (3.7), which relates K_4 to λ and m.

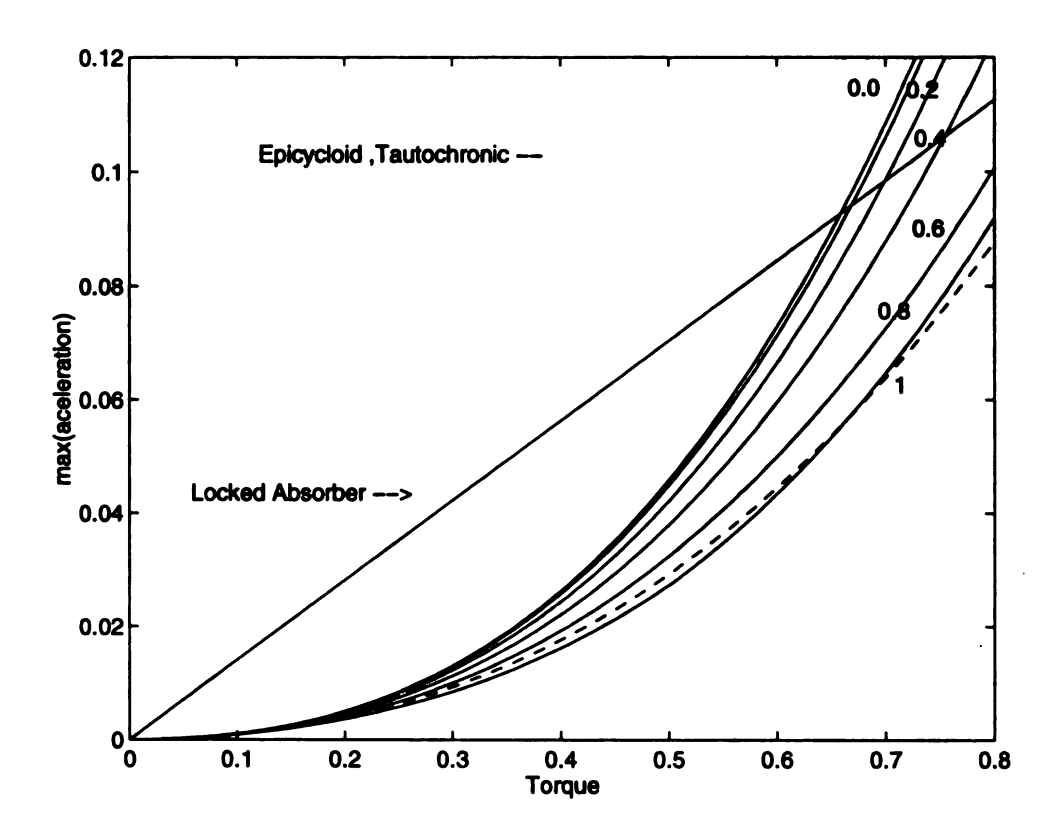


Figure 3.1. Performance of the zero-mistuned absorber paths; Peak angular acceleration vs torque.

Figure 3.1 shows a plot of $|\max(\tilde{\theta})|$ versus Γ_n for the case of perfect tuning, m=n, for the following λ paths

$$\lambda = [0, 0.2, 0.4, 0.6, 0.8, \sqrt{4/5}, 1].$$
 (3.29)

In order to make a meaningful assessment of the performance of a given absorber

path, it is compared against that of the system with the absorber locked at its vertex, which has a peak value, $\max(\bar{\theta}) = \frac{\Gamma_n}{1+b_0}$. This relationship provides a baseline that can be used as a reference to immediately interpret absorber effectiveness.

Figure 3.1 shows a distinct decrease in the maximum acceleration levels as λ varies from 0 (circle) to 1 (cycloid), over all torque levels. A significant difference exists in the acceleration levels obtained from the λ - absorber paths and the locked absorber condition for low to moderate torques, but this difference decreases at higher torques. In fact, for torque levels greater than 0.6, paths with λ values ranging from 0 to 0.4 have acceleration levels greater than the locked condition. The λ paths from 0.8 to 1 maintain a good difference in acceleration levels as compared to the locked condition for torque levels up to (Γ_n) = 0.8, indicating that paths close to the cycloid are good candidates for absorbers, if they are perfectly tuned to the order of disturbance. The path with $\lambda = \sqrt{4/5}$ is the special epicycloid that has the tautochronic property in a radial field for n = 2; it is shown as a dashed curve in Figure 3.1. This path behaves very close to the cycloid and gives acceleration levels slightly lower than the cycloid for Γ_n greater than 0.7.

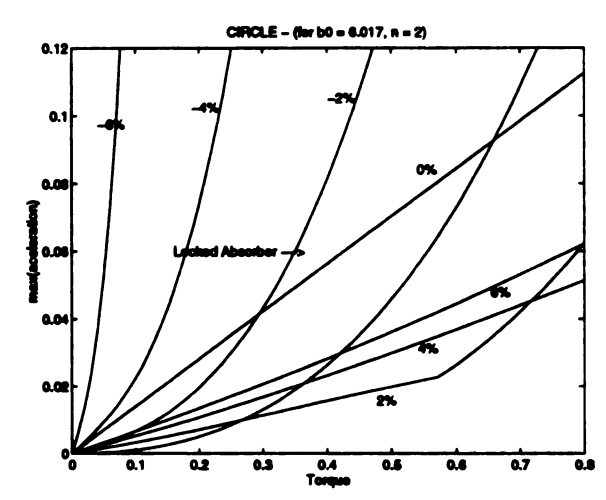
Figure 3.2 and Figure 3.3 depict the peak acceleration versus torque curves for different levels of mistuning for each of the following path types: $\lambda = 0$, 0.6, 1, $\sqrt{4/5}$. The values taken for the mistuning parameter, σ , are

$$\sigma = [-6\%, -4\%, -2\%, 0\%, 2\%, 4\%, 6\%]. \tag{3.30}$$

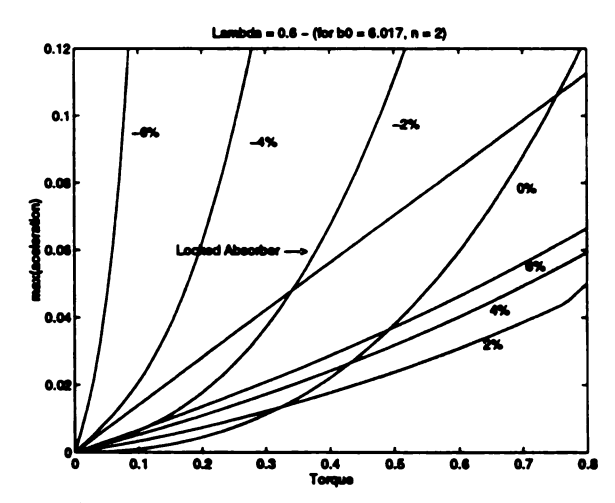
The corresponding m values are calculated from equation (2.20) with n=2 and are

$$m = [1.88, 1.92, 1.96, 2.00, 2.04, 2.08, 2.12].$$
 (3.31)

Figure 3.2(a) depicts the acceleration-torque relationship for the circular paths

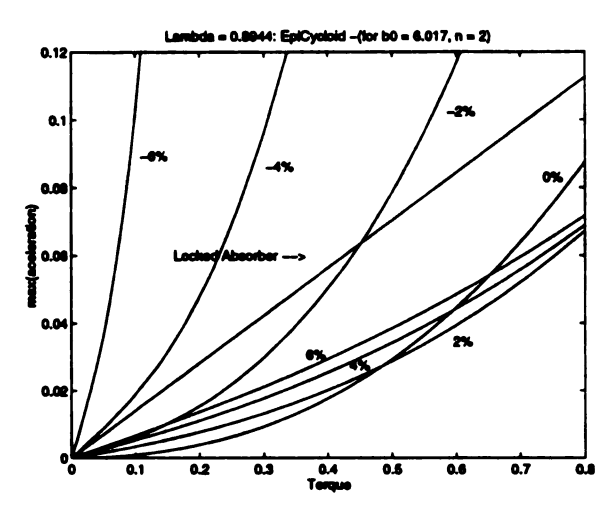


(a) Plot of acceleration versus torque for circular paths.

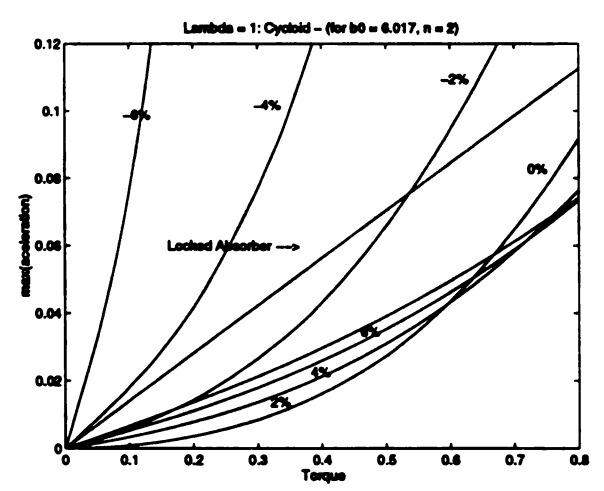


(b) Plot of acceleration versus torque for $\lambda = 0.6$ Paths

Figure 3.2. Performance of the mistuned $\lambda=0,0.6$ paths – acceleration versus torque



(a) Plot of acceleration versus torque for mistuned versions of the tautochronic epicycloid paths



(a) Plot of acceleration versus torque for cycloid paths

Figure 3.3. Performance of the mistuned $\lambda = 0.8944, 1$ paths- acceleration vs torque.

at different levels of mistuning. The acceleration levels increase as the mistuning is varied from zero to negative values. The steep slopes of the curves for negative mistuning indicate that a small increase in torque value causes a large increase in acceleration; this is poor system performance, and in fact the absorbers can actually amplify vibration levels. On the other hand, positive mistuning offers excellent performance, especially for slight mistuning. The accleration curves decrease from 0% to 2% and then increase from 2% to 6% mistuning. The shape of the acceleration curves indicates that the system response becomes nearly linear over a large torque range at higher positive mistuning levels.

Figure 3.2(b) depicts the acceleration-torque curves for the $\lambda=0.6$ paths at different levels of mistuning. This case shows the same character as the circular path case, although there are some differences in the general levels of acceleration at each level of mistuning.

Figure 3.3(a) depicts the acceleration-torque relationship for the $\lambda = \sqrt{4/5}$ (tautochronic epicycloid) paths at different levels of mistuning. Note that the acceleration curves for mistuning $\sigma \in (0\%, 6\%)$ are very close to one another, whereas for mistuning $\sigma \in (-6\%, 0\%)$, they are distinctly apart. Again, when considering the entire torque range, a small level of positive mistuning offers slightly better performance than the perfectly tuned case.

Figure 3.3(b) depicts the acceleration-torque relationship for the $\lambda = 1$ (cycloid) paths at different levels of mistuning. This case shows the same character as the tautochronic epicycloid path, again with slight variations in amplitude for specific mistuning levels.

Figures 3.4 - 3.5 show the effects of mistuning the absorbers at the following selected torque levels: $\Gamma_n = 0.6, 0.4, 0.2$, for paths with $\lambda = 0, 0.6, \sqrt{4/5}, 1$. The torques here represent the mistuning behavior of the system at low, medium and high torque levels.

Figure 3.4(a) shows that for $\Gamma_n = 0.6$ (high torque) the rotor acceleration for all the paths decreases steeply as we approach 0% mistuning from -6% mistuning. The acceleration also initially decreases just beyond 0% mistuning for all paths except the cycloid where 0% is the minimum. The minimum acceleration achieved by the circular path is at 2% mistuning, while for the other two paths the minima lie between 0% and 2%. Also, the circular path with 2% mistuning gives the least overall acceleration for all paths considered at this torque level.

Figure 3.4(b) shows that for $\Gamma_n = 0.4$ (moderate torque) the distinction between the paths is not significant, especially for mistuning levels from zero to 1%. The best performance in this case is offered by the circular and $\lambda = 0.6$ paths, both for about 1% mistuning.

Figure 3.5 shows that for $\Gamma_n = 0.2$ (low torque) λ has very little effect on the response, as expected since the system will operate in a nearly linear manner at this level of torque. Perfectly tuned paths with λ near to unity offer the best performance, by a very small margin.

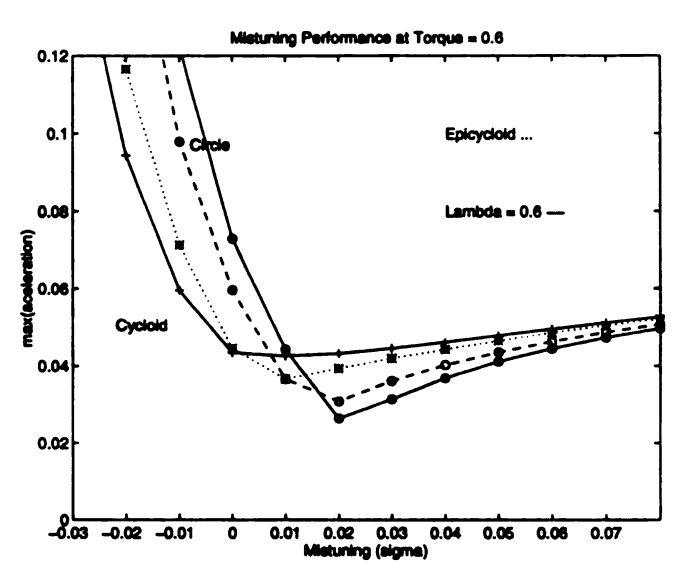
Next, we explain the jump phenomenon results that provide important information about the validity of the results shown in above figures, since they are obtained by the perturbation results.

3.5.2 Numerical Examples for the Jump Phenomenon

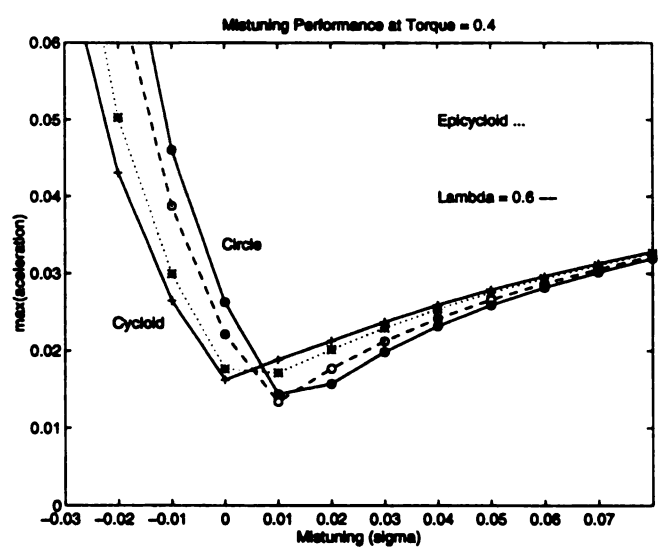
Equations (3.23),(3.26) and (3.27) are used for determining the relationship between the peak amplitude of the absorber s_a and the torque amplitude Γ_n , as well as the associated jump torque, for a given absorber path.

Figure 3.6 shows a plot of s_a versus Γ_n for the case of perfect tuning, m=n, for the following λ paths

$$\lambda = [0, 0.2, 0.4, 0.6, 0.8, \sqrt{4/5}, 1].$$
 (3.32)



(a) Plot of acceleration versus mistuning for $\Gamma_n = 0.6$



(b) Plot of acceleration versus mistuning for $\Gamma_{n}=0.4$

Figure 3.4. Mistuning performance at $\Gamma_n = 0.6, 0.4$

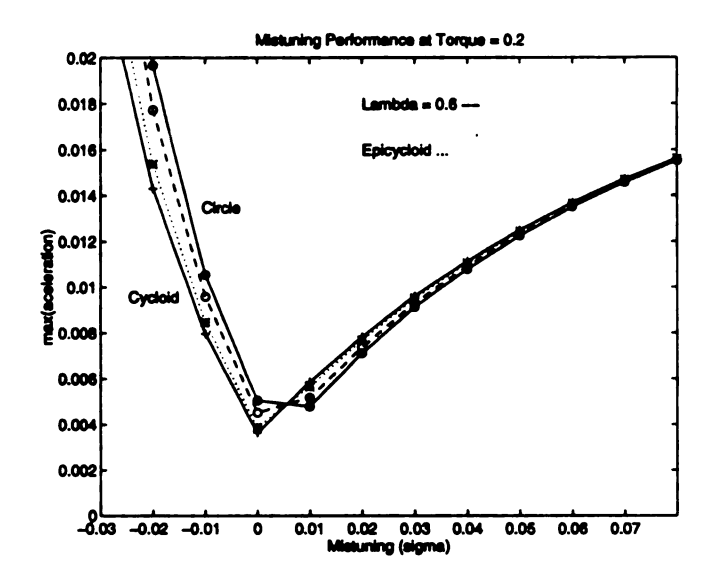


Figure 3.5. Mistuning performance at $\Gamma_n = 0.2$

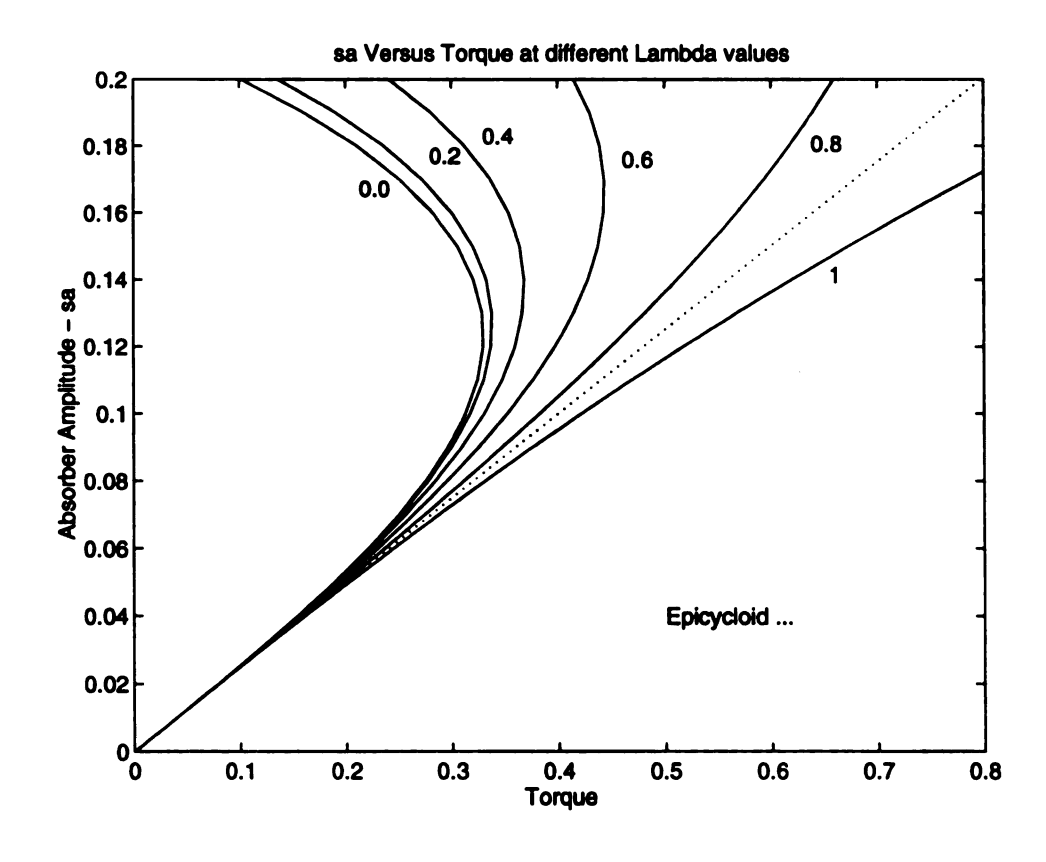


Figure 3.6. Absorber amplitude s_a versus Γ_n at different path λ values

Figure 3.6 demonstrates that the absorber amplitude s_a generally increases with Γ_n . However, for paths $\lambda \in [0, 0.6]$, the absorber amplitude reverses direction in the torque range shown, indicating that there exist multivalued solutions for low levels of Γ_n . The reversal point is the absorber amplitude/torque level at which the jump occurs. The regular perturbation solution is invalid near to and beyond this torque level. Also, note that the jump torque increases as λ is increased, and there is no jump beyond a certain value, indicating that solutions for these paths are valid within the Γ_n range [0,0.8]. Therefore, for perfect tuning, paths like cycloids and epicycloids, i.e. $\lambda \geq 0.8$, offer the best possibility for good performance.

Figure 3.7 and Figure 3.8 depict the absorber amplitude versus torque curves for different levels of mistuning for each of the following path types: $\lambda = 0$, 0.6, 1, $\sqrt{4/5}$. The values taken for the mistuning parameter, σ , are

$$\sigma = [-6\%, -4\%, -2\%, 0\%, 2\%, 4\%, 6\%, 8\%]$$

and the corresponding m values, calculated from equation (2.20) with n=2, are

$$m = [1.88, 1.92, 1.96, 2.00, 2.04, 2.08, 2.12, 2.16].$$
 (3.33)

Figure 3.7(a) depicts the absorber amplitude versus torque relationship for circular paths at different levels of mistuning. The jump torque for negative mistuning $\sigma \in [-6\%, 0\%]$ decreases from 0% mistuning to -6% mistuning. Note that at -6% mistuning, the jump occurs very close to $\Gamma_n = 0$. Also note that for the cases in which a jump occurs, there is large amplitude response curve that exists over the entire torque range. We have not investigated the system performance on this branch, but it is expected to be poor. Also, we have not investigated the dynamic stability of these branches. However, one can guess that the lowermost and uppermost of the

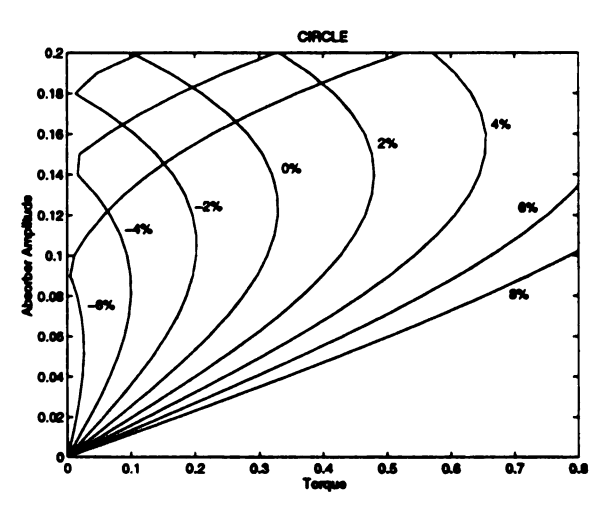
three branches are dynamically stable, while the middle branch is unstable. Thus, as the torque level is increased, at the jump point the solution will suddenly move from the lower branch to the upper one. Similarly, once on the upper branch, when decreasing the torque level the response will follow the upper branch all the way to zero torque. Obviously, such behavior is undesireable. It can be avoided, as is done in practice, by using postive mistuning. As the mistuning is increased from 0% to 8%, the jump torque continues to increase until there is no jump at 6%, 8% mistuning. In fact, the absorber motion is very close to linear at 8% mistuning.

Figure 3.7(b) depicts the absorber amplitude versus torque relationship for $\lambda = 0.6$ paths at different levels of mistuning. This case shows the same character as the circular path case. Note, however, that there is no jump at 4% and the jump torques in this case are higher than for the circular path case.

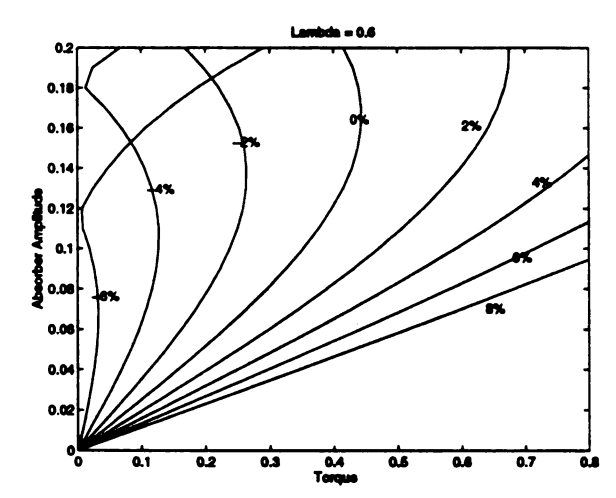
Figure 3.8(a) depicts the absorber amplitude versus torque relationship for $\lambda = \sqrt{4/5}$ (tautochronic epicycloid) paths at different levels of mistuning. Jumps occur at $\sigma = -6\%, -4\%, -2\%$. However, there is no jump at perfect tuning or any values of positive mistuning. The absorber amplitude curves decrease as σ values vary from -6% to 8%. (However, recall that lower absorber amplitude is not the desired goal, and that small mistuning levels minimize torsional vibration amplitudes).

Figure 3.8(b) depicts the absorber amplitude versus torque relationship for $\lambda = 1$ (cycloid) paths at different levels of mistuning. A jump only occurs at $\sigma = -6\%$. Therefore, perturbation results are valid for a wide range of mistuning levels for cycloid paths. Again, absorber amplitude curves decrease as σ values vary from -6% to 8%.

These findings are summarized in a single figure, in which the jump torque levels can be graphically read for a range of mistuning and λ values. Figure 3.9 shows a plot of the jump torque Γ_J verses the mistuning parameter σ , obtained by using equation (3.27) for the values of λ used in this study. Note that the jump torque does not

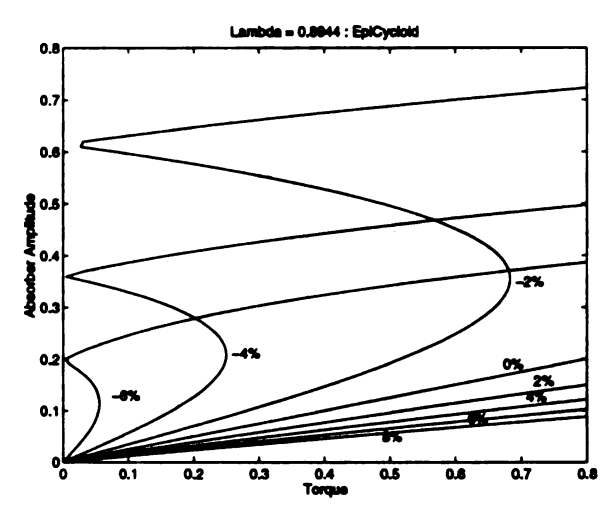


(a) Plot of absorber amplitude versus torque for circular paths.

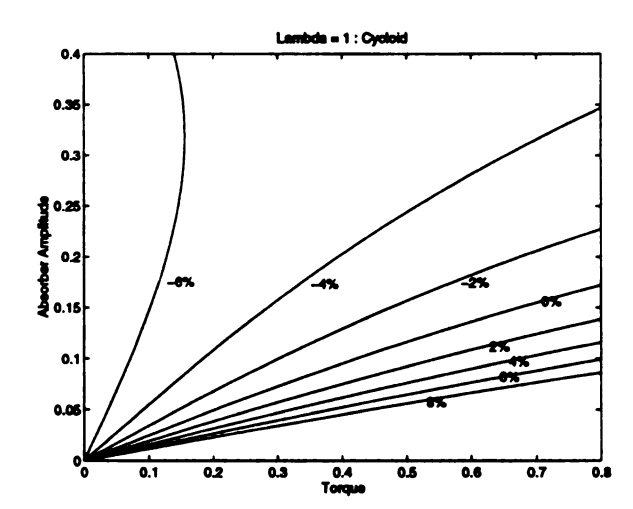


(b) Plot of absorber versus torque for $\lambda = 0.6$ paths

Figure 3.7. Performance of the mistuned $\lambda = 0, 0.6$ paths. Absorber amplitude vs torque level.



(a) Plot of absorber acceleration versus torque for epicycloid paths.



(b) Plot of absorber amplitude versus torque for cycloid paths

Figure 3.8. Performance of the mistuned $\lambda = 0.8944, 1$ paths. Absorber amplitude vs torque level.

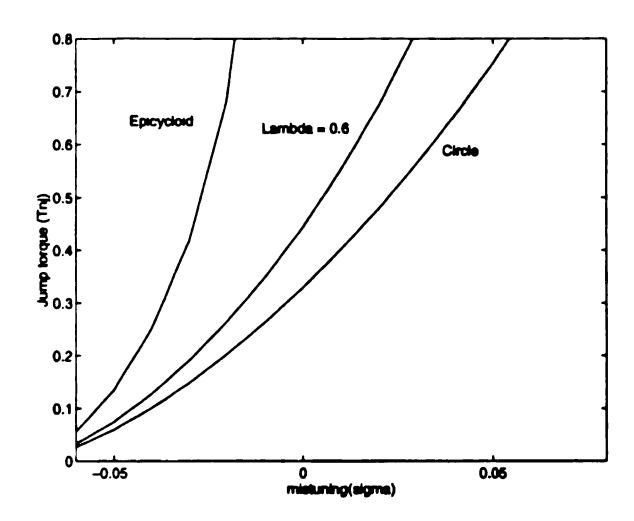


Figure 3.9. Jump torque Γ_J versus mistuning σ at different λ path values

exist for cycloids over the range of mistuning levels shown. Using this figure, one can immediately determine the range of validity of the perturbation results for a given set of parameters. Such information is very useful in evaluating prospective designs.

CHAPTER 4

Numerical Analysis

In this chapter, the numerical method used for solving for periodic solutions of the model equations is described. This approach is rather unusual in that it uses a standard optimization package to find periodic solutions of nonlinear differential equations. The chapter is organized as follows. We first describe the optimization method employed by providing an optimization problem statement with an objective function, constraint functions, and design variables pertaining to the given set of equations. Next, the first-order state equations for the model under investigation are presented. Finally, some numerical results obtained from this approach are used to describe the effects of the system parameters on the response. These are graphically presented and compared with the analytical results obtained in Chapter 3.

4.1 Introduction - Optimization Methodology

The following approach is taken to obtain accurate numerical versions of the periodic solutions of the equations of motion given in equation (2.11). These equations describe the dynamics of a disk with a single absorber. These are reproduced here as they

form the basis of this chapter:

$$ys'' + (s' + g(s))y' - \frac{1}{2}\frac{dx}{ds}(s)y = 0,$$

$$g(s)y^{2}s'' + (b_{0} + x(s) + g(s)s')yy' + \frac{dx}{ds}(s)s'y^{2} + \frac{dg}{ds}(s)s'^{2}y^{2} = \Gamma_{n}\sin n\theta, \qquad (4.1)$$

As is evident from the equations, they represent a non-linear, θ -dependent, conservative set of equations with two degrees-of-freedom, s and y, subjected to a periodic forcing, $\Gamma_n \sin n\theta$. Such non-linear conservative systems with more than one degree of freedom do not generally yield periodic solutions for a given set of initial conditions. In fact, the most generic types of response encountered are quasi-periodic (containing several discrete frequencies) and chaotic. Therefore, in order to obtain the periodic solutions to this set of nonlinear equations for a given set of system and path variables, and for a given torque level, a systematic, iterative procedure is required for identifying the initial conditions that result in periodic solutions. (These solutions are the ones that generally become dynamically stable when damping is added to the system, and thus these are the ones of engineering importance.)

The approach employed in this thesis is one adopted from the solution of design optimization problems. Optimization, as the name suggests, is concerned with the minimization or maximization of functions. These functions can be multivariable, non-linear, time-dependent functions and can be subjected to a set of non-linear or linear, time dependent/independent constraint functions in their variables. There are many optimization algorithms in use today. The algorithm used herein is a MATLAB implementation of Sequential Quadratic Programming Method (SQP). A full description of this algorithm can be found in MATLAB Optimization Toolbox User's Guide [22]. The method essentially involves solving a linear quadratic subproblem (QP) to obtain a descent direction from the initial starting solution. A line

search algorithm, a merit function and the descent direction are then used to obtain a new solution point. A new QP problem is formulated and the process is repeated until the descent direction is zero, which corresponds to the optimum solution.

4.1.1 Optimization Set-Up

In order to obtain periodic solutions to the above set of equations, one imposes the following constraints on the state variables (s, y, and y'),

$$s(\theta) = s(\theta + T)$$

$$s'(\theta) = s'(\theta + T)$$

$$y(\theta) = y(\theta + T),$$
(4.2)

where T represents the θ -period for the solution being sought: $T = 2\pi/n$. The solutions for these dynamic variables comes from the numerical solution from a state-variable representation of the equations of motion, which is given in the next section.

The choice of objective function in this problem is a secondary matter, since the satisfaction of the above constraints is the main goal. Thus, there are many ways one can select an objective function. Some of the possible choices are: the maximum rotor acceleration (or some other norm of the rotor acceleration), or the maximum absorber amplitude (or some other norm of the absorber amplitude). Since the rotor acceleration is generally well-behaved, we choose the maximum rotor acceleration over one θ period as our objective function.

Design variables here refer to the variables that form the solution set of the optimization routine — that is, its output. The solution set is defined as the set of quantities that we are interested in obtaining as a result of the iterative optimization procedure. In the present setting, this set must obviously contain the initial condition of the state equations that results in the desired periodic solution.

Since we are interested in obtaining periodic solutions over a range of torque amplitudes, we have included Γ_n in the solution set, for the reason described here. Because of the highly non-linear components in the state equations, especially at large torque amplitudes, the design variables are highly sensitive to the objective function and attempts to find periodic solutions at a fixed Γ_n value are troublesome (in terms of convergence) and time consuming. For this reason, a modified approach was adopted in which the torque amplitude is included as one of the design variables, that is, in the solution set, with some very specific bounds imposed to achieve our desired goal. This is described in the next section.

Bounds on the Design Variable

With the set of design variables defined, we now set the upper and lower bounds on the design variables. Such bounds are set in order to constrain the design set to a reasonable range and, in the present case, to facilitate the solution. When one has some knowledge about the general location of the solution in design space, one can impose bounds on the design variables that improves the efficiency of the process and the probability of finding a solution. In this spirit, we often utilized the initial states obtained from the perturbation analysis described in Chapter 3 to set the bounds on the initial condition of the state equations.

The selection of bounds on the torque amplitude serves a special purpose here. Since the objective function is generally a monotonically increasing function with respect to torque amplitude, we know that the solution will nearly always be at the upper bound of the torque amplitude. By using a set range of torque amplitudes, one obtains a more robust optimization process and yet can essentially fix the torque level for the solution point by setting the desired value as the upper bound.

Obtaining a Response Curve

By continually incrementing the upper torque bound upward, and with the lower bound set by the previous solution, we can obtain a response curve that can be compared with the perturbation results. This process is initiated by starting at low torque levels where the linearized solution is known to be accurate, and then ratcheting the process up in torque amplitude. The increments in torque level used depend on the resolution desired in the response curve, balanced against convergence considerations (since large increments will lead to convergence problems). This process requires the solution of a well-defined optimization problem for each response point, and it can be carried out for any set of system and/or absorber path parameters.

In order to carry out this procedure, one must have in hand the following: the state equations, the objective function, the constraints, and the bounds defined. To this end, we now turn attention to the formulation of the standard form of the state equations of motion.

4.2 State Equations

Equation (4.1) can be expressed in first order standard form of

$$Az' = F (4.3)$$

where

$$A = \begin{bmatrix} y & s' + g(s) \\ g(s)y^2 & y(b_0 + x(s) + g(s)s') \end{bmatrix}$$
(4.4)

$$z' = \left\{ \begin{array}{c} s'' \\ y' \end{array} \right\} \tag{4.5}$$

$$F = \left\{ \begin{array}{c} \frac{1}{2} \frac{dx(s)}{ds} y \\ \Gamma_n \sin n\theta - \frac{dg(s)}{ds} s'^2 y^2 - \frac{dx(s)}{ds} s' y^2 \end{array} \right\}$$
(4.6)

Defining the states x_1, x_2, x_3 in terms of s, s' and y as follows,

$$s = x_1$$

$$s' = x_2$$

$$y = (1+x_3)$$

$$(4.7)$$

the explicit state equations are given by

$$\begin{pmatrix}
x'_1 & = x_2 \\
x'_2 \\
x'_3
\end{pmatrix} = A^{-1}F$$
(4.8)

Note that x_3 is defined as y-1 so that all states (x_1, x_2, x_3) are zero in the base operating condition. A complete representation of the state equations in terms of the states x_1, x_2 and x_3 can be found in Appendix B.

They have the general form

$$\mathbf{z'} = \mathbf{f}(\mathbf{z}). \tag{4.9}$$

Recall that a prime denotes a derivative with respect to θ .

Equations obtained in this form can now be numerically integrated over any interval of θ to obtain solution traces of the state variables, or combinations of them, as functions of θ . For example, the rotor acceleration is given by

$$yy'(\theta) = \frac{-2\Gamma_n \sin n\theta + 2x_2^2(\theta)x_3^2(\theta)\frac{dg(x_1)}{dx_1} + 2x_2x_3^2\frac{dx(x_1)}{dx_1} + x_3^2g(x_1)\frac{dx(x_1)}{dx_1}}{2(-b_0 + g(x_1)^2 - x(x_1))}.$$
 (4.10)

4.3 Statement of Optimization Problem (in Standard Form)

With the state equations in hand, we now write the optimization problem statement that mathematically summarizes the optimization procedure explained above.

Find
$$\mathbf{x} = \{p_1, p_2, p_3, \Gamma_n\}$$
; $\mathbf{x} \in \Re_4$, that minimizes $\mathbf{f} = -\max_{\theta \in [0, \pi]} yy'(\theta)$, subject to the constraints:
$$h_1 = (\mathbf{z}(\pi) - \mathbf{p})^2 = 0 \quad (periodic \ constraints),$$

$$g_1 = \Gamma_n \leq \Gamma_{high} \quad (upper \ bound \ on \ \Gamma_n),$$

$$g_2 = -\Gamma_n \leq \Gamma_{low} \quad (lower \ bound \ on \ initial \ conditions),$$

$$g_3 = \mathbf{p} \leq \mathbf{p}_{low} \quad (lower \ bound \ on \ initial \ conditions),$$

$$g_4 = -\mathbf{p} \leq \mathbf{p}_{high} \quad (upper \ bound \ on \ initial \ condition),$$
 where
$$\mathbf{p} = \left\{ \begin{array}{c} p_1 \\ p_2 \\ p_3 \end{array} \right\},$$

$$\mathbf{z} = \left\{ \begin{array}{c} x_1 \\ x_2 \end{array} \right\},$$

and z is determined from the state equations, (4.9)

$$z' = f(z)$$
.

Note that Γ_{high} is the torque at which the solution is desired and Γ_{low} is the torque at which the solution was obtained in the previous iteration. p_{low} and p_{high} are the bounds set around the desired initial states, obtained from perturbation results. The first initial guesses for p and Γ_n are taken from the linear solution at low torque amplitude and the subsequent initial guesses are obtained from the solution obtained in the previous iteration.

4.4 Numerical Results

The optimization procedure was employed to produce numerical results which describe the effects of system parameters on the response and also to check the validity of the perturbation results. We return to the example system that was used for the perturbation results in Chapter 3, with n=2 and $b_0=6.017$. We begin with some general observations of the system response and then turn to a more detailed investigation of the system dynamics for a range of m, λ and Γ_n values.

4.4.1 General Observation of the Response

Typical Acceleration Response

Figure 4.1 represents a θ trace of the rotor acceleration over one period for parameter values $\lambda = 0$ (circle) and $\lambda = 1$ (cycloid), for m = n (that is $\sigma = 0$) and $\Gamma = 0.2$ (low torque). Positive acceleration corresponds to the forward θ direction and negative acceleration corresponds to the backward θ direction. Note that the solution is periodic and includes higher order harmonics. In fact, there is a very strong second-

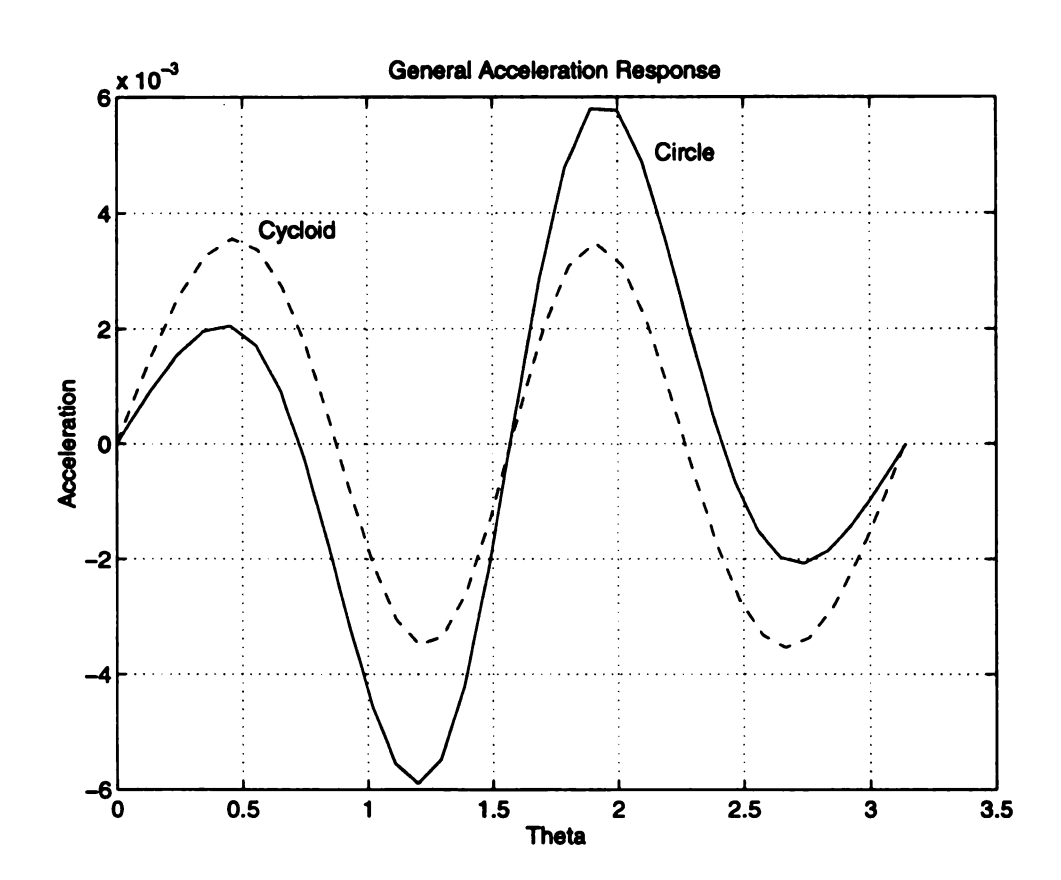


Figure 4.1. General absorber response for cycloid and cicular paths- acceleration vs θ

order harmonic, as expected from the perturbation results. Also note that, due to the zero damping assumption, the acceleration is zero at the beginning and mid-points of the period, exactly where the torque is zero (recall that the applied torque is a sine function [2]). Furthermore, the response is reflection-symmetric about the period mid-point [2]. Therefore, the peak magnitude can be taken from either half-period, using the absolute value. Finally, note that the cycloidal path offers more favorable characteristics as compared to the circular path. These effects are considered in more detail subsequently.

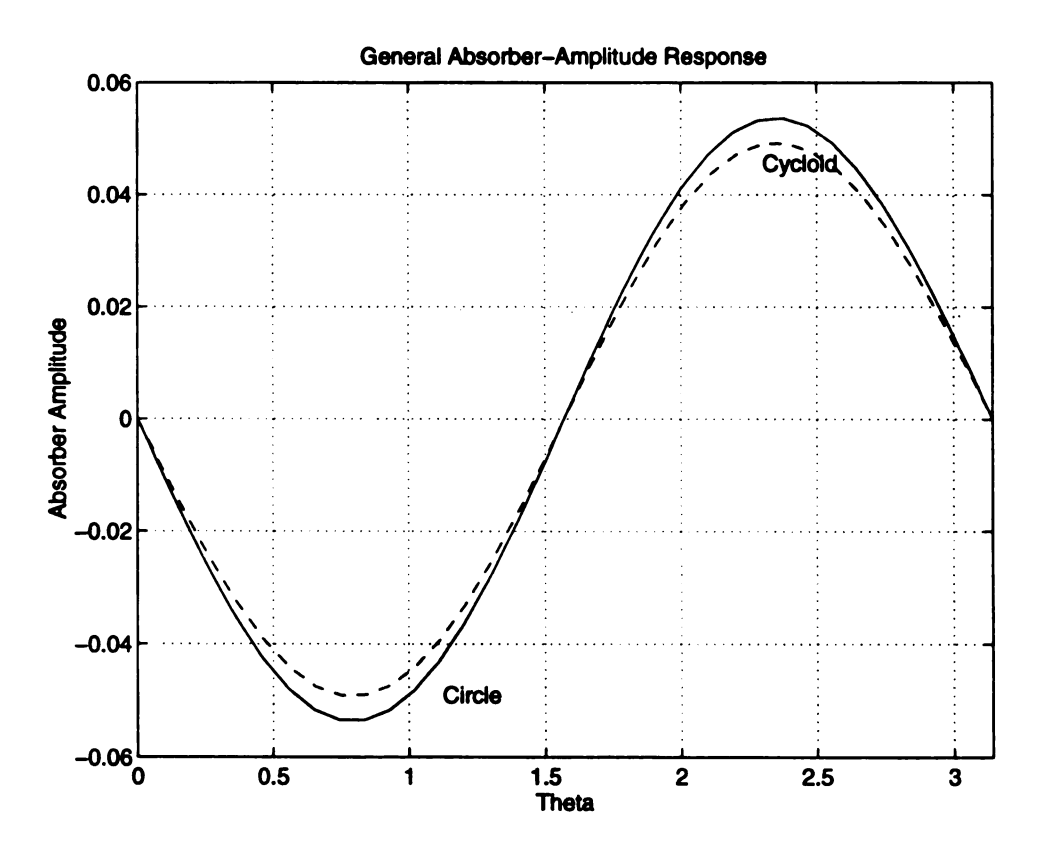


Figure 4.2. General Absorber Response for Cycloid and Cicular paths- Absorber Amplitude vs θ

Absorber Amplitude Response of the System

Figure 4.2 represents a θ trace for the absorber motion over one period for parameter values $\lambda = 0$ (circle) and $\lambda = 1$ (cycloid), for zero mistuning $(m = n \text{ or } \sigma = 0)$ and $\Gamma_n = 0.2$ (low torque). The response is periodic and is out of phase with the excitation torque, which is a sine function in n. Note that the absorber response is nearly a pure harmonic and that higher harmonics are quite small. Also note that the amplitudes for these two paths are nearly the same at this torque level.

We next consider the system dynamics for different λ and m parameters when subjected to a range of torque disturbance amplitudes.

4.4.2 Perfectly Tuned Dynamics

In this section we consider the system response for paths that are perfectly tuned to the excitation torque, that is, m = n (= 2 here) or, equivalently, $\sigma = 0$. Simulations are carried out with $\lambda = 0, 0.6, \sqrt{4/5}, 1$; corresponding to a circle, an intermediate case, the tautochronic epicycloid, and a cycloid, respectively. For each path type, the response was determined for the torque amplitude Γ_n varying from 0.0 to 0.7; the results are shown in Figures 4.3-4.6 in the form of rotor acceleration and absorber response versus θ .

Figure 4.3 depicts the response for the circular path absorber. Responses beyond $\Gamma_n = 0.3177$ were not obtained, as a jump occurs just above this torque level. (In fact, below this value the system possesses two stable solutions, only one of which is shown.) Note that the slope of the rotor acceleration response curve at $\theta = 0$ is negative just before the jump torque level, whereas it is positive away from the jump. The absorber amplitude response shows a steady increase in the amplitude levels from $\Gamma_n = 0.1$ to $\Gamma_n = 0.3177$. In fact, the absorber response grows nearly exactly linearly with respect to Γ_n until just before the jump occurs.

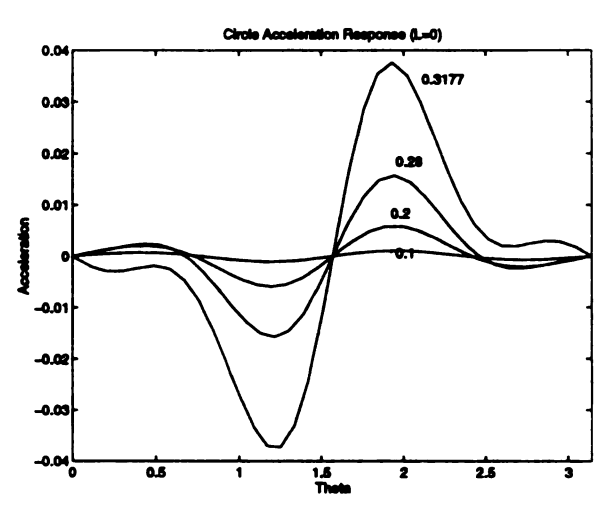
Figure 4.4 depicts the response for a system with an absorber with a $\lambda = 0.6$ path. This case shows the same character as the circular path case, although the jump occurs at the higher torque level of $\Gamma_n = 0.4052$.

Figure 4.5 depicts the response of for a system with an absorber with the tautochronic epicycloidal path. No jump occurs in this case (up to $\Gamma_n = 0.7$). The acceleration and absorber amplitudes show a steady rise from $\Gamma_n = 0.1$ to $\Gamma_n = 0.7$. In this case, the absorber response is very closely approximated by its linearized solution over the entire range of Γ_n values shown.

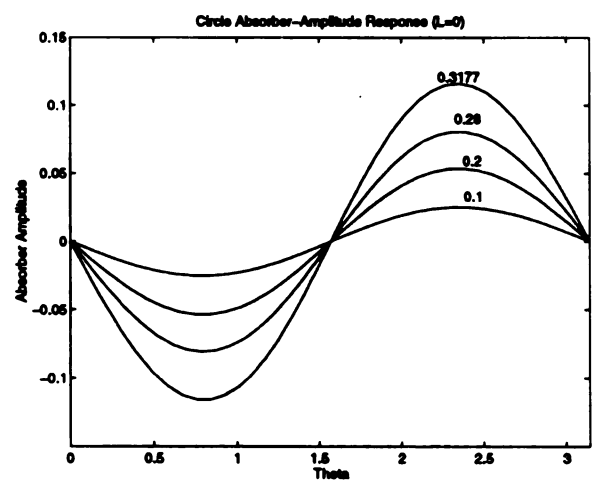
Figure 4.6 depicts the response for a system with an absorber with a cycloidal path. Again, no jump occurs in this case (up to $\Gamma_n = 0.7$), and the acceleration and absorber amplitudes show a steady rise from $\Gamma_n = 0.1$ to $\Gamma_n = 0.7$. However, in contrast to the cases shown before, the first peak of the rotor acceleration response is now greater in amplitude than that of the second peak (during the first half-period). A quick visual comparison at the maximum values of the rotor acceleration for the epicycloid and cycloid cases shows that cycloid gives slightly lower peak values. This shift in the location of the maximum peak value indicates that there exists a path where the two peaks match. Such a condition will offer the optimal path. However, this optimal path will depend on the torque level, and therefore is not of much practical interest. This path is not considered in this thesis, but it can be obtained by investigating paths lying in between cycloid and epicycloid; see [21] for such a study.

4.4.3 Mistuned Dynamics

In this section, absorber paths with $\lambda = 0.0, \sqrt{4/5}, 1.0$ are considered. The paths are mistuned over a range of values of the parameter σ . These values for σ and the corresponding m values are given below

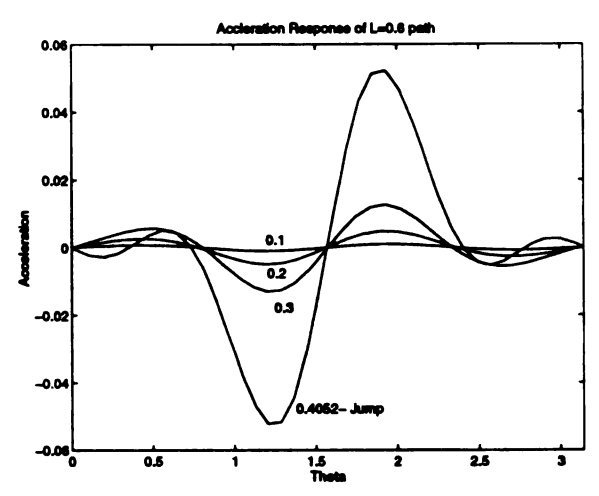


(a) Plot of rotor acceleration versus θ for circular paths for $\Gamma_n = \{0.1, 0.2, 0.28, 0.3177\}$

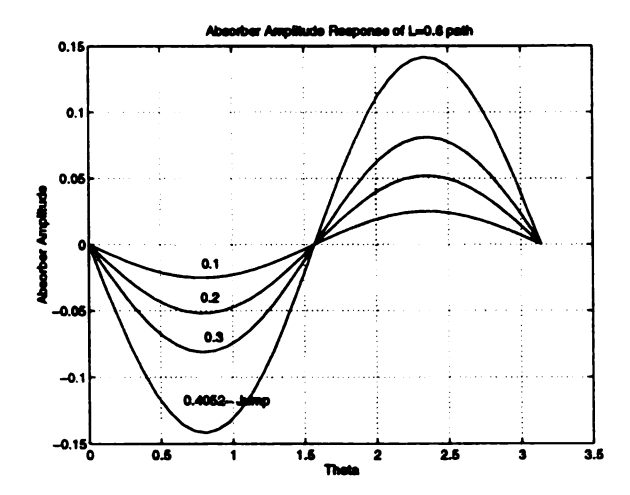


(b) Plot of absorber amplitude versus θ for circular paths for $\Gamma_n = \{0.1, 0.2, 0.28, 0.3177\}$

Figure 4.3. θ - Response of perfectly tuned circular paths

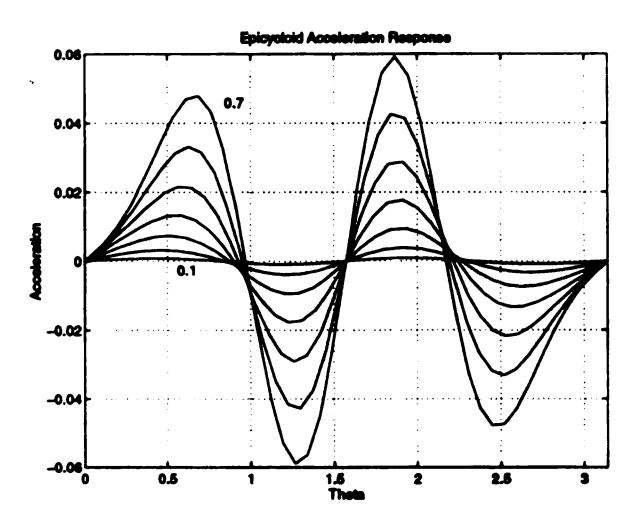


(a) Plot of rotor acceleration versus θ for $\lambda=0.6$ paths for $\Gamma_n=\{0.1,0.2,0.3,0.4052\}$

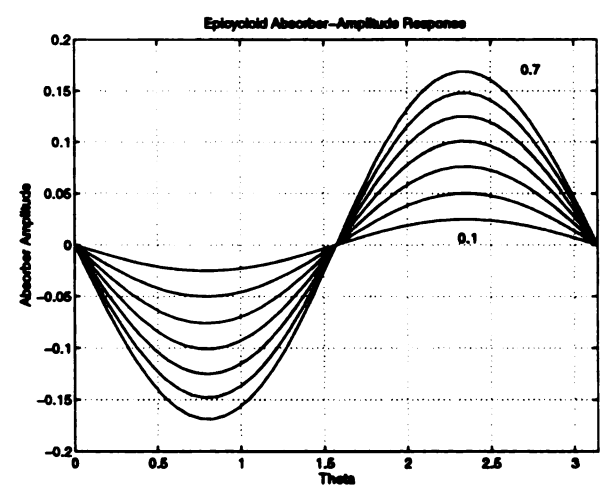


(b) Plot of absorber amplitude versus θ for $\lambda=0.6$ paths for $\Gamma_n=\{0.1,0.2,0.3,0.4052\}$

Figure 4.4. θ - Response of perfectly tuned $\lambda = 0.6$ paths

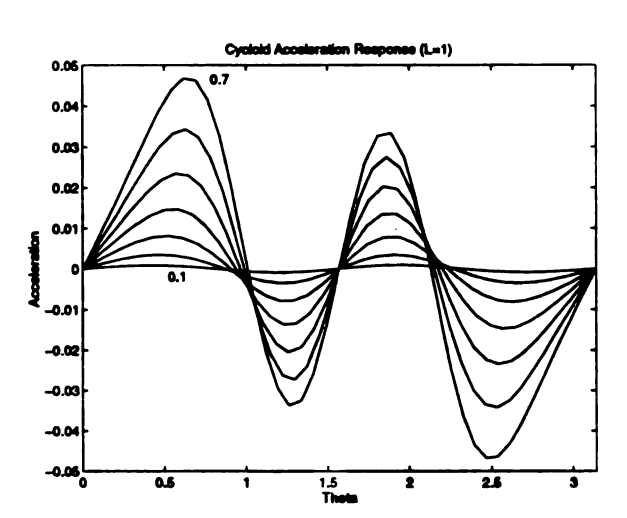


(a) Plot of rotor acceleration versus θ for epicycloid paths for $\Gamma_n = [0.1, 0.7]$

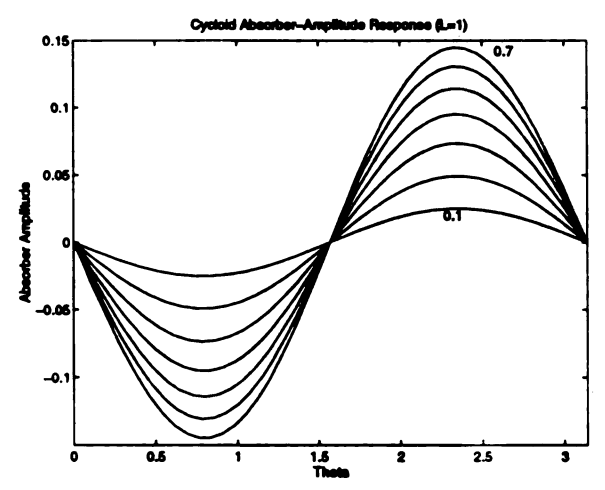


(b) Plot of absorber amplitude versus θ for epicycloid paths for $\Gamma_n = [0.1, 0.7]$

Figure 4.5. θ - Response of perfectly tuned epicycloid paths



(a) Plot of rotor acceleration versus θ for cycloid paths for $\Gamma_n = [0, 0.7]$



(b) Plot of absorber amplitude versus θ for circular paths for $\Gamma_n = [0, 0.7]$

Figure 4.6. θ - Response of tuned cycloid paths

$$\sigma = \{0\%, 2\%, 4\%, 6\%, 8\%\}$$

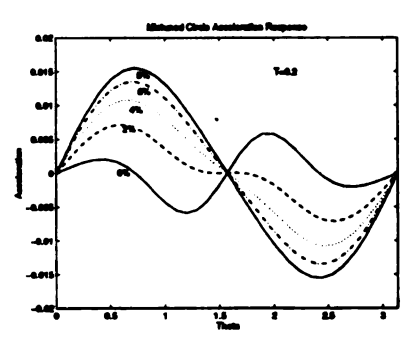
$$m = \{0, 2.04, 2.08, 2.12, 2.16\}. \tag{4.11}$$

The reason for considering only positive values of mistuning is that they generally offer improved performance, whereas negative mistuning nearly always degrades performance; this fact is further demonstrated in section 4.5 wherein the simulation results are compared with the perturbation results. Three levels of torque amplitude are considered for each path: $\Gamma_n = 0.2, 0.4, 0.6$. Figures 4.7-4.9 show the system responses in the form of rotor acceleration for these cases. In all cases the absorber response is nearly a pure harmonic with an amplitude that varies significantly from that predicted by linear theory only when approaching a jump condition.

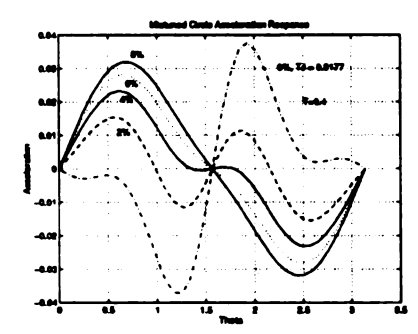
Figure 4.7 depicts the system performance in terms of rotor acceleration for mistuned circular paths. Figure 4.7(a) shows that for $\Gamma_n = 0.2$ (low torque) the maximum acceleration increases as the mistuning is increased. Again the response characteristics change from a dominant second-order harmonic at 0% mistuning to a dominant primary harmonic at 8% mistuning. The shift in the location of the response peak occurs again between 0% and 2% mistuning, suggesting that the best path configuration lies in between these two paths.

Figure 4.7(b) shows that for $\Gamma_n = 0.4$ (moderate torque) there is no solution for 0% mistuning. Recall that this is expected since the jump for 0% mistuning occurs at $\Gamma_n = 0.3177$. However, for the other levels of mistuning shown, the response exists and the maximum acceleration increases with the level of mistuning, from 2% to 8%. Again, the response becomes dominated by the primary harmonic as the mistuning level is increased, although the secondary harmonic persists for larger mistuning levels.

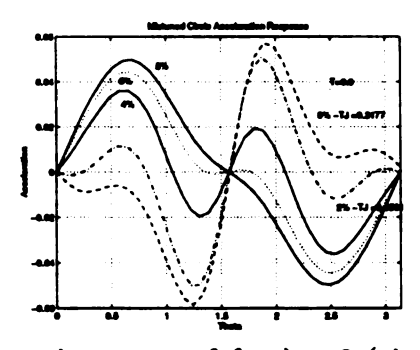
Figure 4.7(c) shows that for $\Gamma_n = 0.6$ (high torque), no solution exists for 0% and



(a) Plot of rotor acceleration versus θ for $\lambda=0$ (circle) paths for $\Gamma_n=0.2$

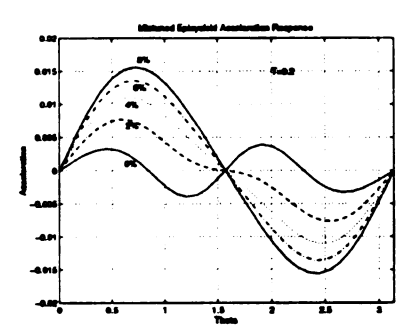


(b) Plot of rotor acceleration versus θ for $\lambda=0$ (circle) paths for $\Gamma_n=0.4$

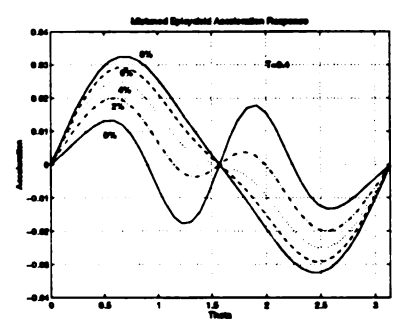


(c) Plot of rotor acceleration versus θ for $\lambda=0$ (circle) paths for $\Gamma_n=0.6$

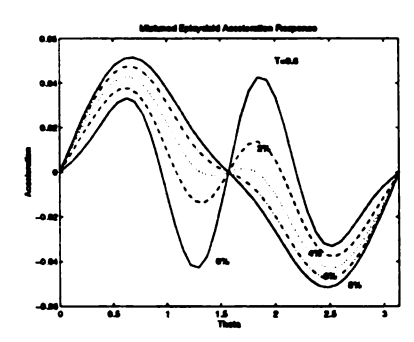
Figure 4.7. θ - Response of mistuned $\lambda = 0$ (circle) paths



(a) Plot of rotor acceleration versus θ for $\lambda = \sqrt{4/5}$ (epicycloid) paths for $\Gamma_n = 0.2$

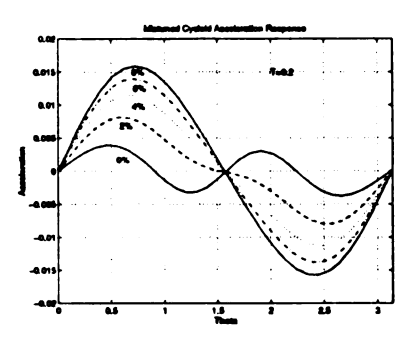


(b) Plot of rotor acceleration versus θ for $\lambda=0.8944$ (epicycloid) paths for $\Gamma_n=0.4$

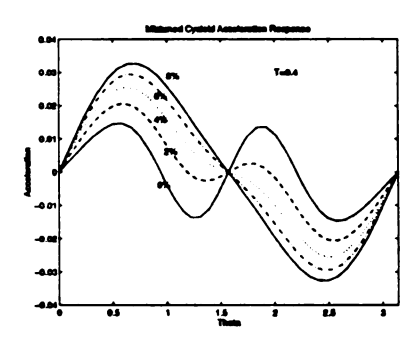


(c) Plot of rotor acceleration versus θ for $\lambda=0.8944$ (epicycloid) paths for $\Gamma_n=0.6$

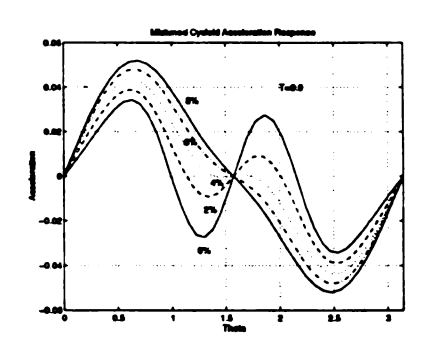
Figure 4.8. θ - Response of mistuned $\lambda = 0.8944$ (epicycloid) paths



(a) Plot of rotor acceleration versus θ for $\lambda=1$ (cycloid) paths for $\Gamma_n=0.2$



(b) Plot of rotor acceleration versus θ for $\lambda=1$ (cycloid) paths for $\Gamma_n=0.4$



(c) Plot of rotor acceleration versus θ for $\lambda=1$ (cycloid) paths for $\Gamma_n=0.6$

Figure 4.9. θ - Response of mistuned $\lambda = 1$ (cycloid) paths

2% mistuning. The jump torque for 2% mistuning is $\Gamma_n = 0.4501$. Responses for the other mistuning levels are qualitatively similar to those for the moderate torque case. However, as expected, the secondary harmonic is even more persistent in this case.

Figure 4.8 depicts the system performance in terms of rotor acceleration for mistuned epicycloidal paths. Figure 4.8(a) shows that for $\Gamma_n = 0.2$ (low torque) the peak acceleration value increases with mistuning and the response characteristics change from having two peaks at (0% mistuning) to just one at (8% mistuning) and from nonlinear (many harmonics) to almost linear (a single harmonic). This is due to the fact that at low amplitudes the system is nearly linear and perfect tuning offers good performance in which the rotor acceleration is dominated by a small second harmonic term. As the level of mistuning is raised, the primary harmonic grows and quickly overcomes the second harmonic.

Figure 4.8(b) shows that for $\Gamma_n = 0.4$ (moderate torque), the maximum acceleration again shows a steady rise as the mistuning is increased. The maximum acceleration at 0% mistuning is actually little less than that of the 2% mistuning. However, it is interesting to note that there is a shift between 0% and 2% mistuning in the peak at which the greatest acceleration occurs. This indicates that there exists a mistuning level between these values which offers the minimum acceleration for this torque level.

Figure 4.8(c) shows that for $\Gamma_n = 0.6$ (high torque), the maximum acceleration is lowest for 2% mistuning and then rises from 2% to 8% mistuning. The maximum acceleration at 8% and 6% mistuning is actually greater than that with zero mistuning. The shift in the largest acceleration peak again occurs between 0% and 2% mistuning, suggesting that the best path lies between these two configurations.

Figure 4.9 depicts the system performance in terms of rotor acceleration for mistuned cycloidal paths. No jump occurs here for the levels of mistuning and torques considered. The maximum acceleration for all the torque levels increases with greater mistuning. Importantly, for 0% mistuning the difference in magnitude for the two acceleration peaks is insignificant at all torque levels, suggesting that this is close to the minimum acceleration path configuration.

4.5 Perturbation - Numerical Comparisons

The analytical results produced by solving the perturbation equations in Chapter 3 and the results produced in this chapter are compared here. These comparisons establish the accuracy of the perturbation procedure which can be used as an important initial design assessment tool for absorber systems.

Figure 4.10 shows the maximum rotor acceleration as a function of torque amplitude for three different paths and a variety of mistuning values. In this figure, results from the analysis are shown as solid curves while the numerically obtained data points are shown as open circles. Note that the analytical results are generally very good, except when the response curves turn past a jump point. The perturbation analysis fails beyond the jump torque value. It is important to note that for cases where the response is nearly a straight line, the linear response provides a satisfactory approximation. However, it is not possible using linear theory to determine where the linear result breaks down.

Figure 4.11 shows numerical and analytical results for the absorber amplitude versus Γ_n at different σ values. The analytical results are obtained from section 3.5.2, which allows one to obtain accurate results beyond the jump. This alternative perturbation approach fixes the large discrepancies between the numerical and the analytical results that are observed in Figure 4.10 when $\Gamma_n \geq \Gamma_J$. These analytical results compare very well with the numerical results and can be used to accurately determine the jump torque (Γ_J) for general absorber path configurations.

Figure 4.12 depicts system responses obtained numerically and analytically in

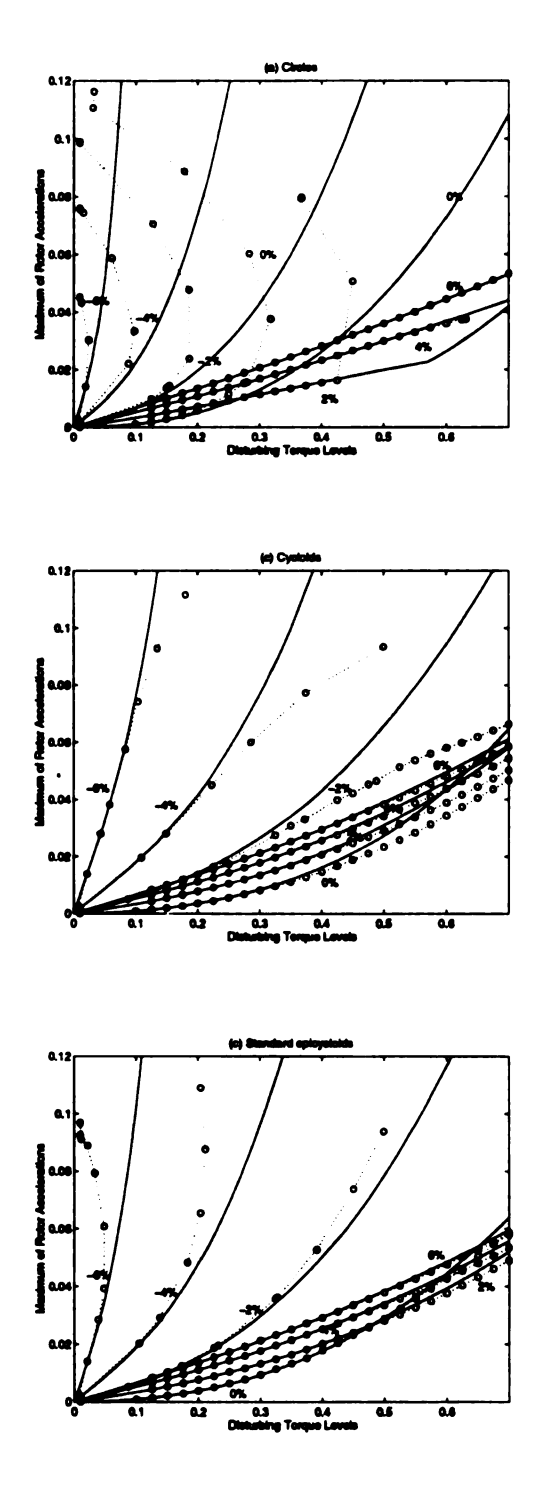


Figure 4.10. Maximum amplitude of rotor acceleration, $\max \left(\bar{\theta} \right)$ versus Γ_n ; solid lines are from perturbation; "o" are from numerical results.

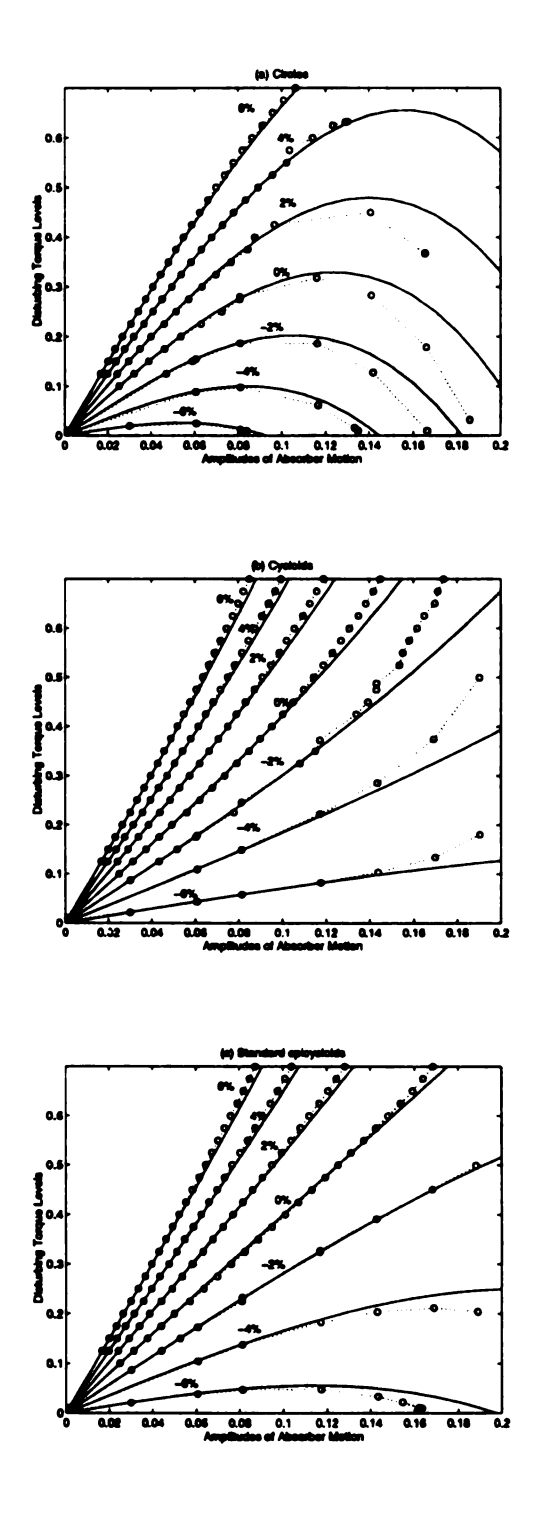


Figure 4.11. Maximum absorber amplitude, $\max(s_a)$ versus Γ_n ; solid lines are from perturbation; "o" are from numerical results.

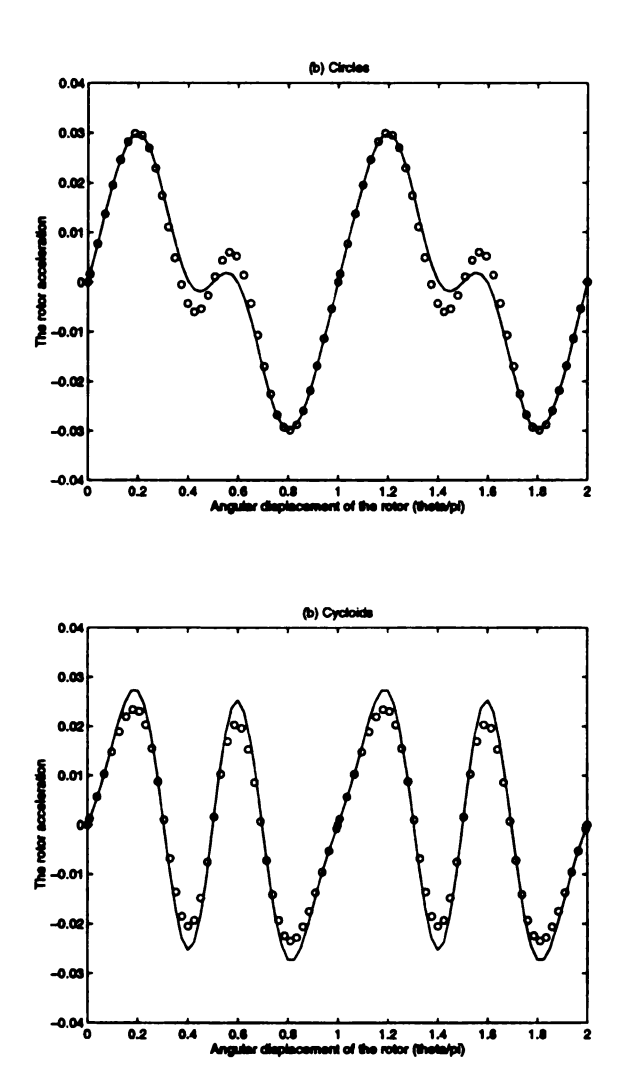


Figure 4.12. Acceleration, $\ddot{\theta}$ vs θ ; solid lines are from perturbation; "o" are from numerical results

terms of rotor acceleration versus θ for $\Gamma_n=0.5$. The responses are for a circular path with mistuning of $\sigma=4\%$, and for a perfectly tuned cycloidal path. This further demonstrates the accuracy of analytical approach.

CHAPTER 5

Discussion and Future Direction for Research

The objective of this investigation was to improve our understanding of the dynamic performance of CPVA systems in terms of the absorber path. The model representing absorber systems was chosen to facilitate the analysis and simulations in order that some general observations could be made regarding the influence of various parameters on the system response. Of particular interest were the nonlinear effects produced by general mistuned paths on absorber system dynamics when subjected to a range of applied torques.

5.1 Design Guidelines

5.1.1 Tuned Path Designs

It has been shown that nonlinear effects are significant over a range of applied torque amplitudes except at very low torques ($\Gamma_n \leq 0.1$) where absorber motions are small. In applications, it is common to design circular paths for the absorbers, as they can provide the required small-amplitude curvature and are easy to manufacture. How-

ever, the nonlinear jump occurring at large absorber amplitudes, even at moderate torque levels, defeats the purpose of the CPVA. Newland [13] provides details about this behavior. The results presented here indicate that for other path configurations (represented here by varying λ from zero [circles] to unity [cycloids]), the jump torque level keeps increasing as we move away from the circle to virtually no jump occurring for paths closer to the cycloid. This is expected and is due to the fact that an increase in the absorber amplitude causes a change in period and this change in its period, if significant, will not maintain the right phasing to absorb the disturbing torque, and will in some cases amplify the disturbing torque. As the path is shifted towards the tautochronic epicycloid (which is quite close to the cycloid for n=2 values of two [where $\lambda = \sqrt{4/5}$] and larger), the absorber period becomes less and less sensitive to the absorber amplitude, thus pushing the jump out to larger and larger torque amplitudes.

5.1.2 Mistuned Path Designs

As has been long known to designers of CPVA systems, the results presented in this thesis indicate that intentional overtuning (positive mistuning) produces great performance enhancements in absorber systems. It was observed that by making tuning adjustments in circular and other paths near the circle, many undesirable nonlinear behaviors (especially the jump) can be completely avoided. The avoidance of the nonlinear jump with positive mistuning is due to the simple reason that absorbers' preferred frequency of motion decreases as their amplitude is increased, and by intentionally overtuning the absorbers, they come into more favorable tuning as amplitudes become large. Both numerical and perturbation approaches also indicate that there is an optimum level of mistuning for a path that will give the best performance for a particular level of disturbing torque. However, it should be understood that this advantage is at the cost of some performance degradation (in terms of rotor acceleration)

at lower torques where a perfectly tuned absorber system offers better performance. This is not crucial, however, since vibration levels at low torque levels are not of importance.

On the other hand, intentional undertuning (negative mistuning) promotes jumps and results in large rotor accelerations for all path configurations. This is expected and is due to the fact that significant frequency discrepancies occur at even smaller absorber amplitudes as compared to the case of zero mistuning.

The net conclusion is that with a slight tuning adjustment, a circular path offers performance comparable to the tautochronic epicycloid and to the cycloid, and it has the added benefit of being easier to implement. One must be careful about the firmness of this conclusion however, as there are limitations in the model employed and ignored effects may be important. These results should be used as rough guidelines and further investigated in light of other significant dynamic effects which are discussed subsequently.

5.1.3 Dynamic Response

The dynamic response of the absorber to the harmonic applied torque is nearly a pure harmonic of order n and is always out of phase with the disturbing torque. This is true over a wide variety of paths that include mistuning. In fact, the absorber amplitude is very well approximated by the linear response (given in equation (3.11)) over a range of torque levels from zero up to nearly the jump torque. This simply follows from the basic kinematics of the system, which do not promote the generation of higher order harmonics in the absorber motion. Due to the kinematics of the system, however, such a harmonic absorber motion does not translate into a harmonic torque on the rotor, and significant harmonics are generated in the rotor acceleration.

The dynamic response of the rotor acceleration has a primary harmonic only when the system is significantly mistuned, but possesses a sizable secondary harmonic in all cases. Also, it is observed that the rotor acceleration is more sensitive to mistuning than to the nonlinear path parameter. Therefore, when developing absorber design specifications, mistuning should always be taken into account.

5.2 Limitations and Future Work

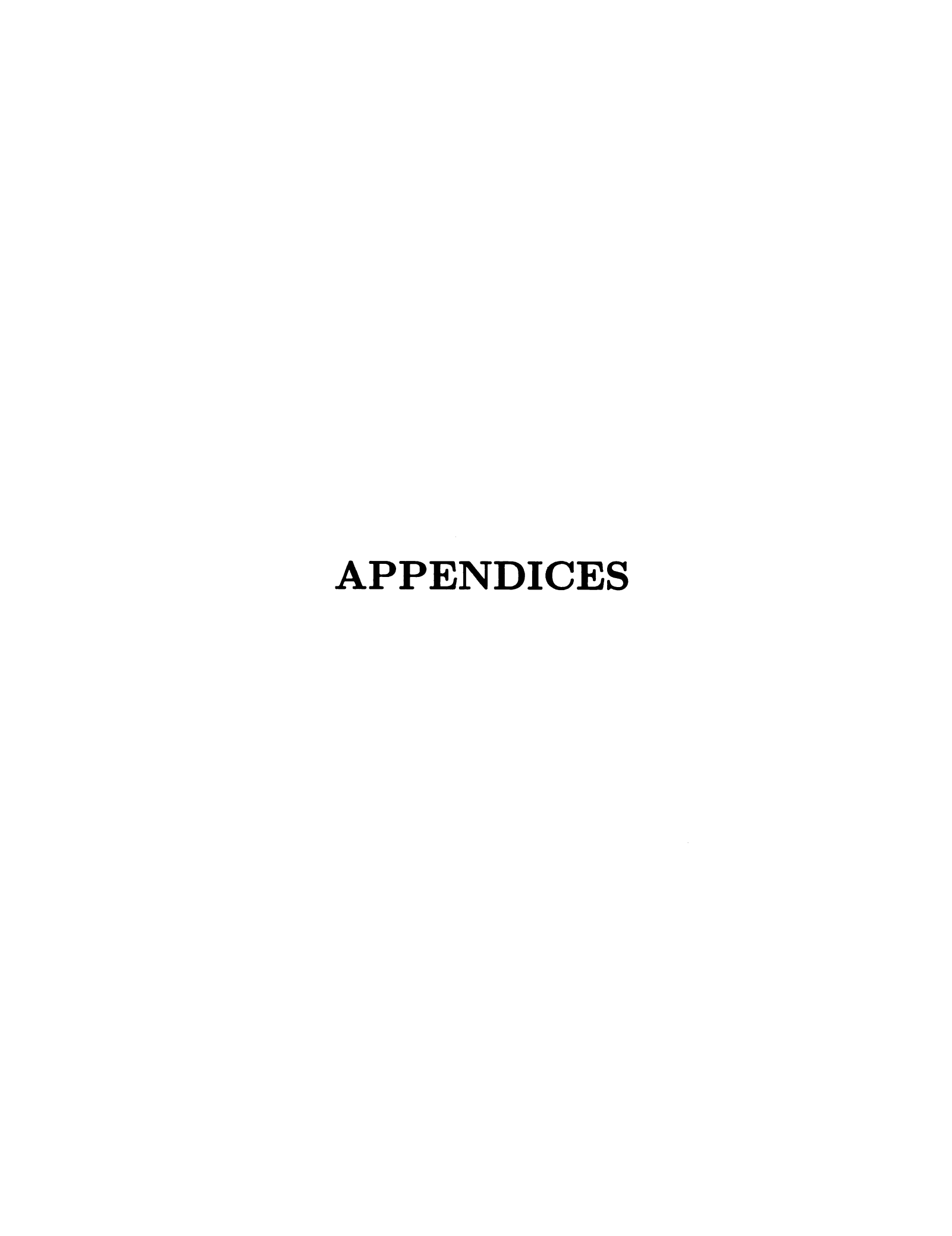
In this section we list a few limitations of the model employed and possible directions for improving the model for future studies. Some known facts about these limitations from concurrent studies are briefly described. Also, additional comments are offered about another absorber system and some speculations about added benefits of using such absorbers.

- Consideration of dissipation. Damping is ignored in this study. It generally has the effect of reducing the performance of absorbers in terms of rotor acceleration, but it also causes a slightly increased torque range for acceptable performance. An improved model including damping effects should be investigated. Also the dynamic stability of the steady state response of the system should be determined, and this result must be obtained from a model with some dissipation.
- Generalized N absorber dynamic system. The dynamic system should be generalized to include the dynamics of a set of N absorbers, even if they are identical. Recent studies have shown that multi-absorber systems can behave quite differently than the present idealized model. Absorbers do not always move in a synchronous manner and studies have shown that beyond certain torque level, the amplitude of one of the absorbers in the set may become quite large. Multi-absorber systems are mostly used for balancing and/or due to restricted space around the rotor. See recent papers for detail [23, 24].

- Consideration of rolling and slipping effects for bifilar absorbers. Bifilar absorbers employ rollers and they may have rolling/slipping effects depending upon the operating and lubrication conditions. However, these effects will be small if their inertia is small relative to that of the absorber mass. Denman includes a detailed analysis of roller dynamics in his study [11].
- Consideration of rotor rigidity. An improved model should include rotor flexibility. Although rotors are generally quite stiff as compared to the absorbers, their effects on the relative motion of the absorbers may be significant. This effect is especially important when more than one absorber is used in the absorber system.
- Inclusion of a complex applied torque model. The applied torque is much more complex than the simple single-harmonic model considered here. It generally includes multiple harmonics and is generated by complex interaction of the inertia forces of engine components, the bearing frictional forces, the gas pressure forces, etc. The paper by Borrowski et al. [10], describes using multiple absorber paths to counteract each individual harmonic of the torque and satisfactory results were obtained using this approach. Similarly, the paper of Lee and Shaw [25] offers a more comprehensive engine dynamics model, incorporating the aforementioned effects. One could (and should) test proposed absorber paths using such a model before building hardware.
- Use of flywheels. Flywheels, owing to their simpler design, can be used in combination with absorber systems. Flywheels also can smooth out irregularities in the torsional system response, but at the expense of reduced system responsiveness and increased weight. The use of absorbers in place of flywheels may be critical for some high-performance applications.

• The subharmonic absorber system. This system, as described in Lee et al. [26] offers absolutely perfect performance by the measures used in this study. It renders zero rotor acceleration over a large torque range using only two absorbers. Its main limitation is that it requires slightly more space for absorber movement. Also, this system is yet to be tested experimentally.

By implementing the above improvements, one can gain a more accurate prediction of the dynamics involved in CPVA systems and have greater insight in solving torsional vibrations problems using these devices.



APPENDIX A

Derivation of Linear Solution

A.1 Linearization in s and θ

Note that from equations (2.9) and (2.10), x and g are functions of s, and since s will be restricted to small values, the following approximations can be used for x(s) and g(s),

$$x(s) = 1 - m^2 s^2$$

$$g(s) = 1 - \frac{(m^2 + m^4) s^2}{2}.$$
(A.1)

Note that here m is given by equation (2.20). These approximations are obtained by expanding the general path function x(s) and keeping terms up to order s^2 . A further account of these approximations can be found in Chapter 3. Note that the above equations are independent of the path parameter λ . By using these assumptions, retaining only those terms linear in s and θ , equations (2.9) and (2.10) can be reduced to

$$\ddot{s} + \ddot{\theta} - \frac{1}{2} \frac{dx}{ds} (s) = 0, \tag{A.2}$$

$$\ddot{s} + (1 + b_0) \ddot{\theta} = \Gamma_n \sin n\theta \tag{A.3}$$

The above equations represent the linearized, dimensionless equations of motion for the system under investigation. The solution for the above equations is developed in the next section.

A.2 Linear Solution

Equations (2.22) and (2.23) can be expressed in the second order standard form of

$$M\ddot{x} + Kx = F \tag{A.4}$$

where

M is the mass matrix,

K is the stiffness matrix,

F is the force vector and

x is the displacement vector, resulting in

$$\begin{bmatrix} (1+b_0) & 1 \\ 1 & 1 \end{bmatrix} \begin{Bmatrix} \ddot{\theta} \\ \ddot{s} \end{Bmatrix} + \begin{bmatrix} 0 & 0 \\ 0 & m^2 \end{bmatrix} \begin{Bmatrix} \theta \\ s \end{Bmatrix} = \begin{Bmatrix} \Gamma_n \sin n\theta \\ 0 \end{Bmatrix}$$
 (A.5)

Note, that there is no damping in the system and the stiffness matrix is only positive semi-definite, indicating the presence of a rigid body mode.

For small amplitude motion, θ can be approximated by,

$$\theta = \tau + \epsilon \tag{A.6}$$

where, $\tau = \Omega t$ and ϵ is a small deviation in θ .

The steady state solution of the system is given by

$$x_{ss} = \begin{pmatrix} \epsilon_{ss} \\ s_{ss} \end{pmatrix} = \begin{pmatrix} A_1 \\ A_2 \end{pmatrix} \sin n\tau = A \sin n\tau$$
 (A.7)

where $A = (K - n^2 M)^{-1} F_0$ and F_0 represents the constant part of the forcing vector.

Substituting equation (A.7) into the equations of motion equation (A.5) and solving for A yields

$$A = \frac{1}{\Delta} \begin{bmatrix} m^2 - n^2 & n^2 \\ n^2 & -n^2 (1 + b_0) \end{bmatrix} \begin{Bmatrix} \Gamma_n \\ 0 \end{Bmatrix}$$
 (A.8)

or

$$A = \frac{\Gamma_n}{\Delta} \left(\begin{array}{c} m^2 - n^2 \\ n^2 \end{array} \right) \tag{A.9}$$

where $\Delta = |K - n^2 M| = n^2 (n^2 b_0 - m^2 (1 + b_0))$

Therefore,

$$\epsilon_{ss} = A_1 \sin n\tau = \frac{\Gamma_n}{\Delta} \left(m^2 - n^2 \right) \sin n\tau,$$
 (A.10)

and the steady-state linearized acceleration, $\ddot{\theta}_{ss}$, is given by

$$\ddot{\theta}_{ss} = \ddot{\epsilon}_{ss} = -n^2 \frac{\Gamma_{no}}{\Delta} \left(m^2 - n^2 \right) \sin n\tau$$

$$= \frac{\Gamma_{no} \left(m^2 - n^2 \right)}{m^2 + b_0 m^2 - b_0 n^2} \sin n\tau. \tag{A.11}$$

Note that this linearized result corresponds to the first term of the non-linear acceleration as obtained by the perturbation method given in equation (3.22). Also, note that it is independent of K_4 (or, equivalently, of λ).

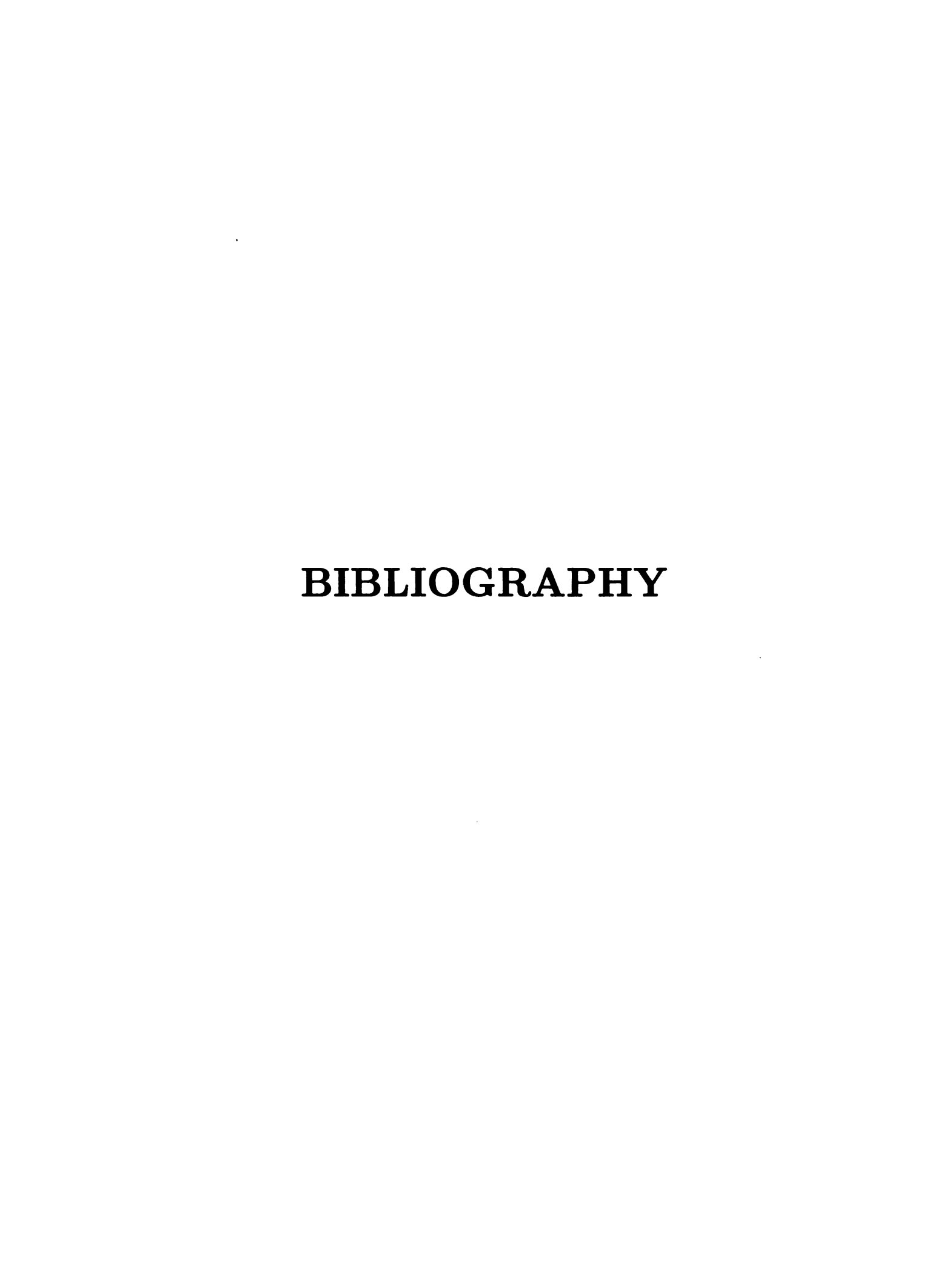
APPENDIX B

State equations for the model

$$x'_{1} = x_{2}$$

$$x'_{2} = \frac{(1+x_{3})^{2} (b_{0} + x_{2}g(x_{1}) + x(x_{1})) x'(x_{1})}{2 (b_{0} (1+x_{3})^{2} - (1+x_{3})^{2} g(x_{1})^{2} + (1+x_{3})^{2} x(x_{1}))} + \frac{(-x_{2} - g(x_{1})) (\Gamma_{n} \sin n\theta - x_{2}^{2} (1+x_{3})^{2} g'(x_{1}) - x_{2} (1+x_{3})^{2} x'(x_{1}))}{b_{0} (1+x_{3})^{2} - (1+x_{3})^{2} g(x_{1})^{2} + (1+x_{3})^{2} x(x_{1})} + \frac{-((1+x_{3})^{3} g(x_{1}) x'(x_{1}))}{2 (b_{0} (1+x_{3})^{2} - (1+x_{3})^{2} g(x_{1})^{2} + (1+x_{3})^{2} x(x_{1}))} + \frac{(1+x_{3}) (\Gamma_{n} \sin n\theta - x_{2}^{2} (1+x_{3})^{2} g'(x_{1}) - x_{2} (1+x_{3})^{2} x'(x_{1}))}{b_{0} (1+x_{3})^{2} - (1+x_{3})^{2} g(x_{1})^{2} + (1+x_{3})^{2} x(x_{1})}$$
(B.1)

Note that g,g',x and x' are functions of x_1 .



BIBLIOGRAPHY

- [1] H. H. Denman, "Tautochronic bifilar pendulum torsion absorbers in reciprocating engines," tech. rep., Ford Motor Company Report #88-08-01, 1988.
- [2] S. W. Shaw and C. T. Lee, "Centrifugal pendulum vibration absorbers," in Smart Structures, Nonlinear Vibration, and Control, Prentice Hall, 1994.
- [3] W. Ker Wilson, Practical Solution of Torsional Vibration Problems, vol. IV, ch. XXX. Chapman and Hall Ltd, London, 3rd ed., 1968.
- [4] J. P. Den Hartog, *Mechanical Vibration*, ch. V. McGraw-Hill Book Company, New York, 4th ed., 1956.
- [5] J. P. Den Hartog, "Tuned pendulum as torsional vibration pendulum vibration absorbers," Stephen Timoshenko 60th Anniversary Volume, pp. 17-26, 1938.
- [6] E. S. Taylor, "Eliminating crankshaft torsional vibration in radial aircraft engines," SAE Journal, no. 38, pp. 81-89, 1936.
- [7] C. F. Taylor, The Internal-Combustion in Theory and Practice, vol. 2, ch. 8. The M.I.T. Press Cambridge, Massachussetts, revised ed., 1985.
- [8] M. H. Hamouda and G. A. Pierce, "Helicopter vibration suppression using simple pendulum absorbers on the rotor blades," *Journal of American Helicopter Society*, vol. 29, pp. 19-29, 1984.
- [9] W. Miao, "Bifilar analysis study Volume I," tech. rep., NASA Report #159227, 1980.
- [10] V. J. Borowski, H. H. Denman, D. L. Cronin, S. W. Shaw, J. P. Hanisko, L. T. Brooks, D. A. Mikulec, W. B. Crum, and M. P. Anderson, "Reducing vibration of reciprocating engines with crankshaft pendulum absorbers," in SAE Technical Paper Series #911876, pp. 73-79, SAE International, Warrendale, PA, 1991.

- [11] H. H. Denman, "Tautochronic bifilar pendulum torsion absorbers in reciprocating engines," Journal of Sound and Vibration, no. 159, pp. 251-277, 1992.
- [12] M. Albright, T. Crawford, and F. Speckhart, "Dynamic testing and evaluation of the torsional vibration absorber," in SAE Technical Paper Series #942519 II, Engines and Drivetrains, P-288, pp. 185-192, 1994.
- [13] D. E. Newland, "Nonlinear aspects of the performance of centrifugal pendulum vibration absorbers," ASME Journal of Engineering for Industry, vol. 86, pp. 257-263, 1964.
- [14] M. Sharif-Bakhtiar and S. W. Shaw, "The dynamic response of centrifugal pendulum vibration absorber with motion-limiting stops," Journal of Sound and Vibration, vol. 126, pp. 221-235, 1988.
- [15] M. Sharif-Bakhtiar, Finite Amplitude Effects on the Dynamic Performance of Centrifugal Pendulum Vibration Absorbers. PhD thesis, Michigan State University, 1989.
- [16] F. R. E. Crossley, "The free oscillation of the centrifugal pendulum with wide angles," ASME Journal of Applied Mechanics, vol. 19, pp. 315-319, 1952.
- [17] F. R. E. Crossley, "The forced oscillations of the centrifugal pendulum with wide angles," ASME Journal of Applied Mechanics, vol. 20, pp. 41-47, 1953.
- [18] M. Sharif-Bakhtiar and S. W. Shaw, "Effects of nonlinearities and damping on the dynamic response of centrifugal pendulum vibration absorber," ASME Journal of Vibration and Acoustics, vol. 114, pp. 305-311, 1992.
- [19] J. F. Madden, "Constant frequency bifilar vibration absorber," tech. rep., United States Patent #4218187, 1980.
- [20] H. H. Denman, "Remarks on brachistochrone tautochrone problems," American Journal of Physics, no. 53, pp. 781-782, 1985.
- [21] C. T. Lee and S. W. Shaw, "A comparative study of nonlinear centrifugal pendulum vibration absorbers," in Nonlinear and Stochastic Dynamics, ASME, volume AMD-Vol.192/DE-Vol.78, pp. 91-98, 1994.
- [22] A. GRACE, Optimization Toolbox. The MATHWORKS INC.

- [23] C. P. Chao, S. W. Shaw, and C. T. Lee, "Non-unison dynamics of multiple centrifugal pendulum vibration absorbers," *Journal of Sound and Vibration*, to appear, 1996.
- [24] C. P. Chao, S. W. Shaw, and C. T. Lee, "Stability of the unison response for a rotating system with multiple pendulum vibration absorbers," ASME Journal of Applied Mechanics, to appear, 1996.
- [25] C. T. Lee and S. W. Shaw, "Torsional vibration reduction in internal combustion engines using centrifugal pendulums," in ASME Design Engineering Technical Conference, volume DE-Vol.84-1, Volume 3-Part A, pp. 487-492, 1995.
- [26] C. T. Lee, S. W. Shaw, and V. T. Coppola, "A subharmonic vibration absorber for rotating machinery," ASME Journal of Vibration and Acoustics, to appear, 1996.

MICHIGAN STATE UNIV. LIBRARIES
31293015818994